7-2-2012

A deployable bottom fed conical log-spiral antenna for CubeSat applications

Anthony Ernest

Anthony J. Ernest
Candidate

Electrical and Computer Engineering
Department

This thesis is approved, and it is acceptable in quality and form for publication:

Approved by the Thesis Committee:

Christos G. Chistodoulou, Chairperson

Mark A. Gilmore

Youssef Tawk

A DEPLOYABLE BOTTOM FED CONICAL LOG-SPIRAL ANTENNA DESIGN FOR CUBESAT APPLICATIONS

BY

ANTHONY J. ERNEST

B.S. ELECTRICAL ENGINEERING
UNIVERSITY OF NEW MEXICO

THESIS

Submitted in Partial Fulfillment of the
Requirements for the Degree of

Master of Science
Electrical Engineering

The University of New Mexico
Albuquerque, New Mexico

May 2012

DEDICATION

to

My wife, for her loving and never-ending support throughout this thesis.

ACKNOWLEDGMENTS

I would like to thank my advisor Christos Christodoulou for giving me the opportunity to get my hands on designing an antenna system. He has sparked my interest during the years of his teaching expertise, which has been an experience I will not soon forget throughout my career.

I would like to thank Youssef Tawk for his support during the final design and testing phase of this project.

I would like to thank Joseph Costantine for his advice and brainstorming during the initial design of this project.

I would like to thank Mark Gilmore for joining my committee on such short notice.

I would like to thank SNL mentors Ken Plummer, Alex Bates, and Tom Atwood, who always gave me a bit of their design experience in every question I asked.

I would like to thank Martha Ernest, Andrea Peterson, Cesar Carmona, and Jordain Sundt for initial editing.

Lastly, I would like to thank Shawn Garcia for his expert skills on this project.

A Deployable Bottom Fed Conical Log-Spiral Antenna for CubeSat Applications

BY

Anthony J. Ernest

B.S., Electrical Engineering, University of New Mexico, Albuquerque, 2010

M.S., Electrical Engineering, University of New Mexico, Albuquerque, 2012

ABSTRACT

The requirements for deployable antenna systems on micro-satellites, specifically on the CubeSat platform, are ever changing. This thesis will address the possible antenna systems that would best be deployed on a CubeSat, with the major focus on the conical log-spiral antenna (CLSA) due to its frequency independent characteristics. The antenna design will then go beyond the published works of the CLSA to introduce a new feeding concept, a bottom fed CLSA. Necessity for this feeding rises out of limited deploying capabilities of the CubeSat platform, which is significantly smaller than the proposed antenna due to frequency constraints. A scaled prototype of the bottom fed CLSA is investigated and optimized. The scaled antenna system is constructed and the results are presented.

TABLE OF CONTENTS

LIST OF FIGURES

LIST OF TABLES

CHAPTER 1

Introduction

A CubeSat is a form of satellite that is in the shape of a standard cuboid or cube. These satellites are part of a multi-university program that was developed through California Polytechnic State University, San Luis Obispo, and Stanford University Space Systems Development Laboratory [1]. Through the initial expansion of the CubeSat program, the main goal was to provide standard guidelines with which a reliable and cost effective space deployment could be achieved. With this ideal in mind and actual space deployment proven, the CubeSat can be manufactured to guarantee many space solutions for a wide variety of consumers. Each unit can have extensively varying mission parameters and from a simplistic view can be broken down into onboard processing and a radio frequency (RF) system. The operational frequency plays the pivotal role of determining the characteristics of the microwave and digital processing sections. Many of these CubeSats have a processing topology which includes a field programmable gate array (FPGA) that can be configured before launch for

mission specific applications. The RF section is greatly dependent on the frequency of operation, where many losses of signal integrity can be encountered due to the response of the microwave system. Thus, the RF system must be designed and simulated over the required frequency band, as no modifications can be made after launch. Therefore, an RF system must be thoroughly and systematically tested to avoid any chance that the system will not perform as required after launch.

In light of the great frequency dependence of the microwave scheme on a CubeSat system, the goal of this thesis is the design and development of an antenna system prototype that can be used with a standard CubeSat satellite. Specific parameters of this thesis have been dictated and will be adhered to throughout the design process. Such antenna parameters to be designed are gain, half power beam width (HPBW), polarization, input return loss (RL), and bandwidth. As the CubeSat has payload restrictions on weight, the size of the antenna becomes an issue due to additional deploying and supporting structures. Therefore, in addition to the design parameters, an overall goal is the reduction of the radiating element dimensions. The motivation is the design of a challenging antenna system that has defined parameters, where the overarching goal is deployment on the CubeSat platform. The required antenna parameters and definitions must be introduced and are presented in the following sections.

1.1 Required Antenna System Parameters and Definitions

The requirements for the antenna design were prearranged and will be presented in this section. Main parameters of the design include gain, polarization, frequency bandwidth, and input return

loss. Other aspects of the design, such as HPBW, were not given and will remain an open constraint. The following is a list of the requirements along with their respective definitions.

1.2 Gain ≥ 5dBi

The gain is the figure of merit between the directivity and efficiency of an antenna. Efficiency of the antenna is defined by the losses within the antenna and at the input or feed [2]. The total efficiency factor can also include the input RL; however this parameter will be included within its own description due to its already given requirement. The efficiency of the antenna within this thesis will consist of conduction and dielectric efficiencies, which are represented as e_c and e_d respectively. As these two efficiencies are inseparable numerically or experimentally, they can be lumped into a single variable. The antenna radiation efficiency can be represented linearly as:

$$e_0 = e_c e_d$$

The efficiency factor describes how well a structure transforms electrical energy into propagating waves, whereas the directivity describes the direction in which the far-field waves are to propagate. Within an elevation and azimuthal angles, represented as θ and φ respectively, the antenna gain can be described as:

$$G(\theta, \varphi) = e_c e_d D(\theta, \varphi) = e_0 D(\theta, \varphi)$$

Evaluating gain in terms of decibels relative to an isotropic radiator, as dBi, the following equation is derived:

$$G(\theta,\varphi)_{dBi} = 10 * log_{10}\left(e_0 D(\theta,\varphi)\right) = (e_0)_{dB} + D(\theta,\varphi)_{dBi}$$

Where $(e_0)_{dB}$ is the efficiency in decibels ranging from -∞ dB to 0 dB. The respective percentage efficiency is thus 0.00% and 100%. Therefore the gain in dBi is related to the directivity by the subtraction of the total internal antenna losses. As an example an antenna that has an efficiency of 50% will have a gain that is 3dB lower than that of the directivity. When presenting directivity within this thesis it must be noted that antenna efficiency will be taken into account when simulating and measuring radiation patterns. The process by which the gain is determined within the simulation domain will be explained further in Chapter 4.

1.3 Circular Polarization

Polarization of an antenna is defined as the image that the maximum of the electric field vector traces as a function of time when observed from behind the transverse electromagnetic wave [18]. That is, the polarization describes the shape and orientation of the electric field vector as it propagates in time. Polarization is distinctly elliptical with two special cases being linear and circular. For elliptical and circular polarization (CP), the sense of rotation describes the direction the electric field vector turns, which can be right-handed or left-handed. The axial ratio (AR) is the ratio of the major and minor axis and ranges from 1< AR < ∞, where unity represents a circularly polarized wave with equal major and minor axis and infinity represents a linearly polarized wave with the disappearance of the minor axis. The sense of polarization will not specifically be discussed; rather the axial ratio will be presented in the form of decibels, with the range dictated by the 3dB beam width.

A common figure of merit for the polarization loss between circularly and linearly polarized antennas is ½ or -3dB. This does not correlate to an axial ratio value of 3dB, rather the CP and linearly polarized antennas represent zero and infinity values of axial ratio, respectively. Therefore another merit must be given for the polarization loss between two antennas, where one is assumed to be perfectly circularly polarized, an axial ratio of zero, and another that has an axial ratio of 3dB. Values of axial ratio and polarization loss have already been investigated and a simple graph for determining them is seen in Figure 1.1 [4]. By drawing a line from the transmitting antenna's axial ratio to the receiving antenna's axial ratio, the intersection point on the maximum polarization axis represents the corresponding polarization loss. From a RHC antenna to linear antenna the loss is 3dB, as expected. From a RHC antenna to RHC antenna with AR=3dB the maximum loss is 0.2dB. Therefore the 3dB AR beam width is associated with a low polarization loss.

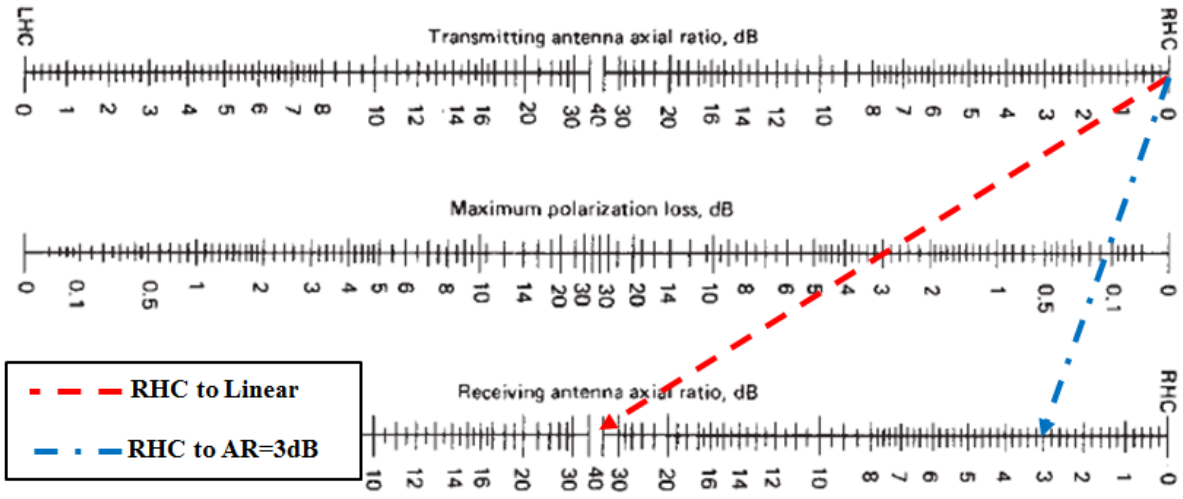

Figure 1.1 A graph to determine the polarization loss with respect to the axial ratio value of two antennas [4].

1.4 Input Return Loss ≤ -10dB

The input RL, as previously mentioned in antenna efficiency, is the metric of impedance mismatch at the antenna terminal and the feed network. When measuring RL from an antenna it has one distinct meaning: the amount of power returning from the antenna related to incident power. An inferred meaning is that the power delivered to the antenna successfully is being radiated, which is not always true. Since the antenna is being considered as a load in the network, the power can be dissipated within the load and not radiated. This percentage is directly related to the antennas radiation efficiency and dictates how much of the non-reflected power is translated into a propagating wave. All of these efficiency terms will form the antenna gain.

In a perfectly matched system, all of the power is transferred from transmission line to load and thus the return loss is zero or -∞dB. The mismatch can be calculated as the reflection coefficient of the load, Z_L, and the transmission lines characteristic impedance , Z_0, as:

$$\Gamma = \frac{Z_L - Z_0}{Z_L + Z_0}$$

The reflection coefficient can also be expressed as the ratio of the return to incident voltage at the input port. In terms of S-parameters, the reflection coefficient is equal to S11, which is also expressed as the same ratio of voltage [19]. S11 is related to the return loss by the following expression:

$$RL = 20\log(|\Gamma|) = 20\log(|S11|)$$

As RL is in terms of power, the logarithmic base is multiplied by a factor of two. When measuring the RL on a network analyzer, it is often replaced with the power equivalent of the S-parameters. The most common relation is simply replacing the transmission or reflection loss/gain by the appropriate S-parameter. For instance, the RL will be given as S11 and the insertion loss (IL) or gain will be given as S21. By the definition of the S-parameters this designation would be incorrect; however this representation is simply in terms of power instead of voltage. The relation between the S-parameters and power based on the definition of time averaged power, which is the square of the voltage over twice the resistance. Given a two port network, as seen in Figure 1.2, the incident, reflected, and transmitted power are represented as:

$$P_{inc} = \frac{|V_1^+|^2}{2Z_0}; \quad P_{trans} = \frac{|V_2^-|^2}{2Z_0}; \quad P_{refl} = \frac{|V_1^-|^2}{2Z_0}$$

Where the ratios of the power are defined as:

$$\left.\frac{P_{trans}}{P_{inc}}\right|_{V_2^+=0} = \left.\frac{\frac{|V_2^-|^2}{2Z_0}}{\frac{|V_1^+|^2}{2Z_0}}\right. = |S21|^2; \quad \left.\frac{P_{refl}}{P_{inc}}\right|_{V_2^+=0} = \left.\frac{\frac{|V_1^-|^2}{2Z_0}}{\frac{|V_1^+|^2}{2Z_0}}\right. = |S11|^2$$

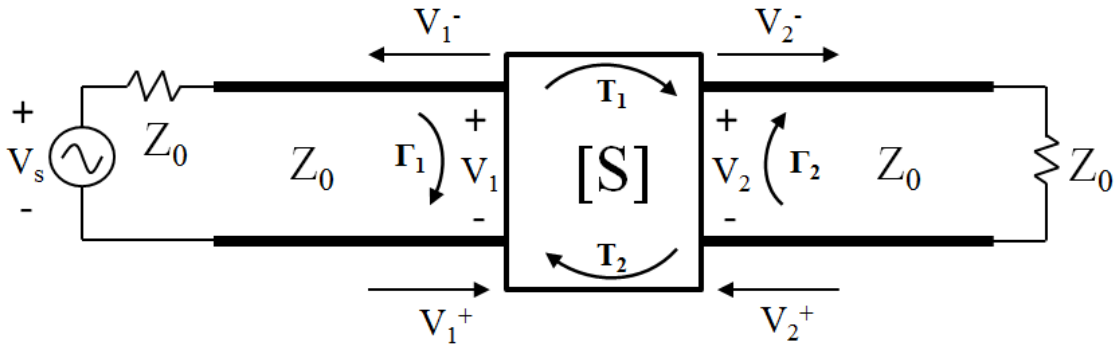

Figure 1.2 Representation of the S-parameters as a two port network.

With the S-parameters defined in terms of power, in can be seen that the return and insertion loss equations are the logarithmic of the above power equations. As it is easier to define a cascaded system in terms of power, the convention of keeping the S-parameter as power will be kept with the knowledge that it is strictly the ratio of power and not voltage. The tools that use this convention of the S-parameters within this thesis include network analyzers and simulation tools. Therefore, to keep with convention, the following definition will be used throughout this thesis as:

$$S11_{power} = RL = 20\log(|\Gamma|); \quad S21_{power} = IL = 20\log(|T|)$$

1.4.1 Frequency Bandwidth = 220MHz – 380MHz

Determining the operational frequency of the antenna is paramount to design. As most antenna sizes are based on wavelength, the corresponding frequency and bandwidth must be known. The bandwidth within this thesis will be defined by the percentage bandwidth over which the antenna characteristics are stable. Impedance matching, as previously discussed, is designed to be less than -10dB for the input RL. The percentage is defined as the difference between the lower (220 MHz) and higher (380 MHz) band edges over the center frequency. The range of the percentage bandwidth is from 0% to 200%, with the upper range only possible when the lowest frequency is zero. The percentage bandwidth can also be classified into three different categories. These categories are narrowband, wideband, and ultra-wideband (UWB). As narrowband and wideband overlap, the boundary with which UWB systems are classified as $BW\% \geq 20\%$. In equation form the percentage bandwidth is expressed as:

$$BW\% = \frac{f_2 - f_1}{f_c} * 100\%$$

Where $f_c = \frac{f_2 + f_1}{2}$ and can be replaced in the above equation. This substitution leads to the band edge form of percentage bandwidth:

$$BW\% = 2\frac{f_2 - f_1}{f_2 + f_1} * 100\%$$

In terms of the given lower band (220MHz) and upper band (380MHz), for this thesis, the percentage bandwidth is determined to be:

$$BW\% = 2\frac{f_2 - f_1}{f_2 + f_1} = 2\frac{380MHz - 220MHz}{380MHz + 220MHz} * 100\% = 53.3\%$$

From the given bandwidth of the system requirements, the antenna system will need to have an UWB frequency response. That is, across the entire band the radiation pattern, input matching, polarization, and other parameters need to remain consistent. The reasoning for consistent antenna characteristics is to ensure proper functioning across a bandwidth as well as being able to guarantee other aspects such as data rates. If a communications channel is dependent across a frequency band, then the robustness of the channel would be a function of the antenna parameters, as discussed within the above gain section, and the channel itself. With CubeSat, the path would generally be Line of Sight (LoS), with the assumption that atmospheric losses are dominant in comparison to terrestrial communication which would have fading and multipath environments [11].

1.5 CubeSat Antennas

Many antennas have been proposed for the CubeSat, which range from size reduced patch antennas to wire based antennas. Patch antennas offer many integration benefits, which include non-deployable mounting. Frequency and bandwidth are major concerns with the patch antennas, as the dimensions are a restrictive feature. Wire antennas have been proposed as easy to deploy, however their bandwidth and single polarization becomes limiting factors in high performance systems. The next chapter will cover a background investigation of possible antenna systems that are practical with the given requirements.

CHAPTER 2

Background Antenna Investigation

From the given requirements, an investigation into possible antenna structures that could be deployed from a CubeSat is investigated. The investigation is directed at wire antennas, as they have been the prominent choice for deployment on the CubeSat platform [4]. From wire antennas the choices become limited, as many integrated systems employ the use of antennas on printed circuit boards. A wide variety of antennas can be realized from planar structures, however the size of the planar antenna and the deployment becomes an issue with the relative size of the standard CubeSat (10x10cm, 10x30cm, and 10x60cm) [1]. This aspect will be discussed within the section including microstrip patch antennas. The major condition is the deployable aspect of the antenna; as the size, due to the rigorous requirements, will be the

dictating factor of the antenna design. Noting this constraint, possible antenna types and configurations that match the given requirements are explored.

2.1 Microstrip Patch Antennas

The microstrip patch antenna consists of a layered structure with a metal ground plane, substrate, and an etched metal top layer. The top layer dictates the matching and radiation characteristics of the antenna. The required parameters of the needed antenna that can be met include circular polarization, impedance matching, and directivity [10][2]. Circular polarization can be achieved in a square patch with dual feeds orthogonal to each other, which are also 90° out of phase. The phase difference needed is to put each x- and y-component of the polarization in the same path, where a 90° hybrid would accomplish this feature. Another method for obtaining circular polarization is by placing the feed along the diagonal of the rectangular patch. The currents along the patch would then be directed in both the x and y directions. Proposed patch antennas include minimizing the size to fit on a single CubeSat platform [6]. Center frequency must be always taken into account with patch antennas, as the size is directly related.

Operating at frequencies around the 300MHz regime, a quick calculation of a rectangular microstrip will be demonstrated. If the resonant frequency, f_r, is 300MHz, the length of a rectangular patch in the dominant TM_{010} is described as λ /2 [2]. Assuming that the material has an $\varepsilon_r = 3.5$, and neglecting fringing effects for brevity, the length of the patch is approximately:

$$L = \frac{c}{2f_r\sqrt{\varepsilon_r}} = \frac{300}{2(3)\sqrt{3.55}} m = 41cm\ (16.41in)$$

Including fringing will cause the physical length to decrease, depending on the height of the material. This would mean that the effective dielectric constant would determine the actual length with the fringing effects fully accounted for. The typical percentage bandwidth for these patches is 15% – 25% which does limit the capability for the required application [10]. However, the calculated length above is a simple representation which does not account for the amount of a ground plane needed under the patch. Using $\lambda/2$ as a standard unit of measure, the largest dimension of the proposed antenna is approximately 50cm (19.6in) and 40 cm larger than the 1unit CubeSat (10cm x 10cm). Many aspects of a planar design would need to be reconciled, especially when deployment is concerned. High permittivity reduces the electrical size of the rectangular patch, but this could lead to milling tolerance issues and an unrealizable design without the cost of small transmission line modeling. As the design is most likely larger than the CubeSat, a non-standard material would be required to "unwrap" a planar design. Therefore, planar designs will not be considered for deployment options due to their size and extensive modifications to the material that would inevitably be needed.

2.2 Helical Antenna

The Helical antenna is a wound wire tread that forms a helix, as shown in Figure 2.1. There are two typical modes of operation for the helical antenna, which are the normal and axial mode. The modes are related by the circumference with respect to the wavelength of operation [10]. The normal mode has a broad side far-field pattern that is similar to that of a dipole. The axial mode has an end-fire far-field radiation pattern that has maxima along the axis of the helix.

More modes do exist for the helical antenna; however the axial mode is exclusively discussed within this section.

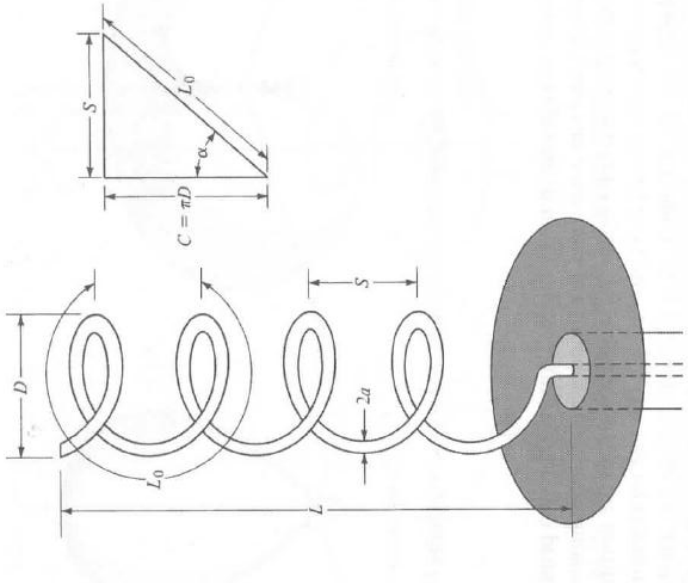

Figure 2.1 Helical antenna schematic and associated parameters [2].

The axial helical antenna is an ideal candidate for the CubeSat program, as it exhibits circular polarization, wide bandwidth, and a directive beam. Glasser and Krauss determined the empirical characteristics of the input impedance to be approximate of the following relation within ±20% [7]:

$$R = 140\frac{C}{\lambda_0}$$

From Figure 2.1, the parameters of the helical antenna are *D*, *S*, *C*, and α which represent the diameter, coil spacing, coil circumference, respectively. The dimensions of the end-fire helical antenna are based on the number of turns needed to achieve desired axial ratio. For the

axial mode the following relations between circumference, coil spacing, and pitch angle must follow:

$$^3/_4\,\lambda_0 \le C \le {}^4/_3\,\lambda_0 \quad or \quad {}^3/_{4\pi}\,\lambda_0 \le D \le {}^4/_{3\pi}\,\lambda_0$$

$$S \cong {}^{\lambda_0}/_4; \quad \alpha = \tan^{-1}\frac{S}{C}; \quad HPBW = \frac{K_B\lambda_0^{\frac{3}{2}}}{C\sqrt{NS}}; \quad Gain_{losses} = \frac{K_G NS}{C^2{\lambda_0}^3}$$

Where the equation for the pitch angle, α, can be simplified with the approximate values of *S* and *C* into the inequality $10.6° \le \alpha \le 18.4°$. Table 2-1 and Table 2-2 give an idea of how large the helical antenna would be with respect to a CubeSat platform. The center frequency from 220MHz to 380MHz is calculated as 300MHz or 1.0m (39.3in) wavelength in free space. Choosing an N=5 will result in an axial ratio < 1dB and will be used for the demonstration. Table 2-1 shows the antenna dimensions such as height, diameter, and circumference. Table 2-2 shows the input impedance, lossless gain, and HPBW at the center frequency of 300MHz and band edges of 220MHz and 380MHz.

Table 2-1 Dimensions of helical antenna at center frequency of 300MHz

Frequency (MHz)	Wavelength (m) [in]	Height (m) [in]	Diameter (m) [in]	Circumference (m) [in]
300	1 [39.3]	1.25 [49.2]	0.31 [12.2]	1 [39.3]

Table 2-2 Parameters of helical antenna at center frequency and band edges

Frequency (MHz)	Impedance (Ω)	Gain (dB)	HPBW (degrees)
300	140	12.73	46.5

220	186	8.90	71.6
380	112	16.47	30.2

From the calculated values, it can be seen that the gain and HPBW vary over the bandwidth. Depending on the tolerances needed across the bandwidth, the helical antenna may vary too much in gain and HPBW. With minimal support structures the height becomes a problem and must be reduced. This can be done with eliminating the number of turns which also reduces the axial ratio. The amount of loss is dependent on the polarization loss factor with respect to that axial ratio, as previously discussed in the antenna requirements section. Contingent on the number of turns, the polarization loss factor could be calculated with respect to the resultant axial ratio. For a single beam the antenna needs a ground plane that is typically $3\lambda/4$. The ground plane and the antenna would then need to be deployed together to prevent a back lobe from radiating the CubeSat. The helical antenna is an ideal choice for the CubeSat program, where it has already been modified into other forms such as a hemispherical helix. The choice is thus reliant on the variance of the antenna parameters over the 56% bandwidth and the resultant adverse effects over the bandwidth to the specific application in question.

2.2.1 Tapered Helix

The tapered helix is an attempt to gain a larger impedance bandwidth by tapering the turns in a linear fashion. Depending on the taper and the size of the turn it scales across the desired frequency band. Designing this antenna would require the circumference of the upper and lower frequency bands to be at the largest and smallest portion of the antenna. That is, the top most

turn would have a circumference related to the upper frequency and vice versa for the lower frequency. The design equations for the taped helical antenna are similar to end-fire helical antenna and will not be repeated here for brevity.

2.3 Frequency Independent Antennas

Frequency independence is employed by closely following the scaling of the geometry and angles such that each component along the antenna acts as a locally periodic structure [10]. Frequency independent antennas can take many forms, however the definition remains the same for any structure that is frequency scaled to meet the rigorous bandwidth demands. Two types of frequency independent antennas will be presented in the following sections.

2.3.1 Log-Periodic Antennas

Log-periodic antennas have structures that vary as a logarithm of the frequency band within which the antenna is defined. These types of antennas can take many forms and the focus should remain on wire for ease of deployment. A prime example of this antenna is the log-periodic wire dipole antenna which is comprised of two sets of crisscrossed monopoles. Spacing and monopole size is related to the growth rate τ.

Design of this antenna system is typically about a known and optimized spacing factor that is related to a specific growth rate [9]. Active regions of the antenna depend on the growth rate and the angle of the increasing antenna size, which almost forms a conical outline about the

increasing monopoles. Each monopole has a length of λ/4 with respect to each frequency component. With respect to the growth rate, each monopole is scaled across the frequency band about this constant. Therefore the total size is dependent on the frequency bandwidth, the growth rate, and relative spacing. The largest component is at the lowest frequency of 220MHz, where the size is a total of λ/2 or 68 cm (26.7 in). Textbook designs typically have the gain in the range of 8 - 15dBi [10].

The log-periodic dipole does not have any considerations for circular polarization. However circular polarization can be achieved with an identical section that is orthogonal to the first. The two sets would need a 90° hybrid between the two orthogonal antennas and balanced feeding for both. This effectively doubles the deployment requirements for the antenna. This type of antenna could be compressed, but the stability of the supporting structures is unknown. The log-periodic antenna characteristic has the possibility for deployment on the CubeSat platform, but needs considerations for CP and deployment structures.

2.3.2 Spiral Antennas

Spiral antennas are frequency independent and are usually formed with two or more arms that are identical but shifted 180° apart from each other. The focus within this section is going to be on the equiangular, or Archimedean spiral. The frequency independence is defined by the innermost and outermost radii of the spiral, where the lowest frequency is defined by the outer radius and the highest frequency is defined by the inner radius.

The spiral antenna is circularly polarized over the defined frequency bandwidth with strictly real input impendence. However, a limiting feature of most planar spirals is the bi-

directional main lobes where a null is located in the plane of the spiral. An absorber is usually placed on the backing of these types of planar spirals to reduce the backfire radiation towards the feeding structure [10]. This reduces the efficiency of the antenna to approximately fifty percent.

A method to direct the radiation in one main lobe has produced the equiangular spiral on a conical structure. This gives light to the conical log-spiral antenna (CLSA) that has circular polarization, wide impedance bandwidth, and a possibility for size reduction [13]. Unlike the log-periodic dipole, the CLSA has characteristics of circular polarization without the need for a secondary antenna or hybrid system. Deployment of this antenna can be done by direct compression of the associated antenna wire or by rotation. All of these factors make the CLSA an ideal candidate for deployment on the CubeSat platform and matches the required antenna parameters. Therefore, this type of antenna should be explored further for possible use on the CubeSat platform; this is presented in Chapter 3.

CHAPTER 3

Conical Log-Spiral Antenna

In the investigation of frequency independent antennas, it was found that an antenna could be designed using these techniques. While the percent bandwidth is not excessively large for the application in this thesis, some consisting of 100% or even upwards 150%, the overall size could be reduced when using bounded constraints defined by frequency band edges. The main influence within this area of study is the formation of differing structures that an equiangular, or log-spiral, could be structured to fit. Many applications of this idea can take place, with spirals placed on a pyramid, hemisphere, or paraboloid [10]. These works are based within the notion of other similar antennas, one of those being the previously investigated helical antennas. The conical form is built into some helical antennas, where the tapering of the wire is enforced to improve bandwidth. However these forms rely on tradeoffs between the radiation pattern, axial

ratio, and overall antenna size, which are not as heavily weighted in frequency independent antenna applications.

Dyson experimented with placing the log-spiral on a conical structure for reducing the backward radiation associated with the planar equiangular spiral [13]. Much experimental data is credited to Dyson's work, which paves the way for designing antennas such as the CLSA without the use of back absorbers. In discovering many aspects of the radiation from the structure, the most prevalent to this thesis is the reduction in size while maintaining the needed frequency independence. With overall size being the limiting factor, further investigation into this antenna system is warranted.

3.1 Antenna Parameters

To gain control of the radiation pattern the equiangular spiral was placed on a conical structure. In doing so, several variables are created that give way to degrees of freedom in design. As presented with the planar spirals, there exist various modes that are dependent on the number of spiral arms and feeding phase between them [13]. The omnidirectional radiation pattern for higher order modes is not desirable to the present application. Using a two arm log-spiral, where the principal mode is a single beam, the parameters of the conical structure and the spiral are to be discussed, through focus on their effects of the far-field radiation pattern. Choosing a dual arm spiral, the feed between the arms is differential or balanced, being 180° out of phase with each other. Like all two arm antennas this ensures that currents are balanced. How this antenna will be fed is discussed within Chapter 7, which goes into balanced feeding and how this aspect is accomplished.

3.2 Governing Equations

The conical log-spiral is governed by a modification to the equiangular spiral. With the spiral resting on the face of a cone, the equation must be projected into three dimensions. Starting with the equiangular spiral equation, the conical log-spiral is defined as the radial vector that is a function of the angle φ. This relation can be expressed as:

$$\rho(\varphi) = \rho_0 e^{\beta\varphi}$$

Where,

$$\beta = \frac{\sin(\theta_0)}{\tan(\alpha)}$$

The other parameters seen are θ_0 and α. These represent conical angle from the z-axis and wrap angle, respectively. Figure 3.1 shows the coordinate system for the conical log-spiral with the given variables. From the governing equation, as φ increases the radial distance, which lies on any point of the spiral arm, traces out the equiangular spiral on the conical face. The initial distance from the apex of the cone, ρ_0, is found to be:

$$\rho_0 = \frac{\sin(\theta_0)}{r_u}$$

Finding the starting point depends on upper radius of the cone, or as defined in the equation above r_u. The lower radius, or r_L, defines the lower truncation of the cone that does not affect the radiation pattern and can be traced by the spiral arms at an φ_{max} angle. The upper and lower radii are dependent on the upper and lower frequency ranges. These are defined by the active

region, which changes with respect to wrap and conical angle. Through the measurements of Dyson, the upper and lower radii will be defined by a desired beam width.

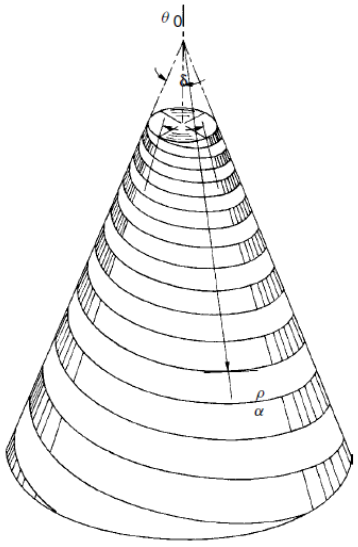

Figure 3.1 The CLSA with related parameters [15]

3.3 The Active Region

Before going into designing the antenna, the wave characteristics and propagation along the spiral arms must be discussed. The log-spiral antenna is in a slow-wave configuration within areas that are outside the "active region" of the antenna. Inside the active region the slow-wave nature changes into a fast-wave, where the wave changes directions and is backfired toward the vertex of the cone. The slow-wave area is made up of tightly bound surface waves, which continue as the propagation constant is increased. These tightly bound waves are coupled into a space wave travelling toward the vertex and the propagation constant becomes complex [13]. The complex propagation constant is the driving force that allows the traveling backfire wave that leads to the radiated power toward the apex of the cone forming a single directed beam.

The active region of the antenna is defined as the region with which the antenna radiates. This area is also where the far-field characteristics are determined. Naming the active region of the antenna across a frequency bandwidth is what reduces the size of the antenna. The upper and lower frequency band edges are defined by the user and highly depend on the radii at upper and lower diameters of the spiral, respectively. Dyson found that a negligible change in the radiation pattern was found on the lower end of the conical structure where the near-fields from the antenna were reduced by 10dB to 15dB from the maximum measured within the active region. Reductions of the near -field on these lower parts of the antenna lead to the conclusion that the truncation of the turns can be made with minimal changes to the far-field pattern and axial ratio, of the designed lower frequency band edge. Further truncations to this region greatly impacted the HPBW and axial ratio. Thus, the lower portion of the active region is mapped and can be called a_{15}^{+} and a_{10}^{+} for the near-field reduction of 15dB and 10dB, respectively. For compact antenna sizes with a slight distortion to the main beam on the lower frequency end, the a_{10}^{+} can be used in lieu of the a_{15}^{+} region, as the a_{10}^{+} value represents a smaller lower cone radius.

Similar to the lower truncation, an upper truncation region can be used to further reduce the size of the antenna. The upper region that held major consequences in the far-field pattern was at a value of 3dB down from the maximum measured near-field value within the active region of the antenna. This corresponds to the higher frequency range of the designed bandwidth. Any removal of the antenna structure beyond the 3dB point results in extreme pattern degradation. This point of 3dB near -field reduction at the conical apex is named a_{3}^{-}.

With the regions of the active region defined, the relation to the cone size is needed. It is essential to the design of the antenna to accurately identify the active region for the antenna parameters. These parameters include spiral wrap, conical angle, and the bandwidth of

operation. The radius of the cone is described in terms of the operating wavelength, or more conveniently as a ratio of the upper and lower truncation regions over wavelength. Finding specific radii with relation to the measured active region is the defining role of the design engineer. Aspects of how these features are related to the far-field pattern are discussed in the following sections.

3.4 Antenna Input Impedance

The input impedance of the antenna is dependent on the width of the spiral arms. A general consensus has been formed with the CLSA, where very small and large widths have been found to be approximately 320Ω and 80Ω respectively [13]. These impedances also depend on the conical angle, where as it increases the impedance increases as well. The conical angle can be increased until the arms are in a single plane and the theoretical impedance approaches that of a equiangular spiral antenna of 60π or 189Ω. As the governing equations do not take this facet into account, the impedance will have to be optimized during simulation modeling.

3.5 Antenna Parameters and the Active Region

Control of the beam is through the manipulation of the spiral wrap and conical angles. This beam control is directly related to the active region of the antenna, where all of the radiated field characteristics are formed. With this knowledge, how the size of the active region governs the far-field becomes the question of design. Therefore, two variables, spiral angle α and conical angle θ_0, dictate the far-fields from the log-spiral antenna and will be explored here.

The relationship between the spiral angle and conical angle in terms of the average half power beam width can be seen in Figure 3.2. Note that when θ_0 approaches 90° the structure becomes a planar spiral. From the figure it can be seen that regardless of the conical angle, the spiral wrap describes the level of directivity the antenna will have. As the wrap angle increases, the directivity increases and thus by a reciprocal fashion the HPBW decreases. The nature of the directive beam with a larger spiral angle is due to the periodic structure, or active region, being extended to cover a greater number of elements. That is, the wrap angle increase leads to a shifting of the active region, where the upper radius increases and the lower radius decreases. This relation is only seen for wrap angles above 70°, otherwise the relationship is reversed and the lower radius of the active region gets larger while the upper radius gets smaller. This change describes the switching of directional to omnidirectional modes for the antenna. The conical angle also plays a role with the shifting of the active region along the antenna, with the larger angles giving way to a wider angle for the active region and thus a broader main or omnidirectional beam. All of these parameters relate back to the size of the active region with respect to the antenna, which should not be surprising.

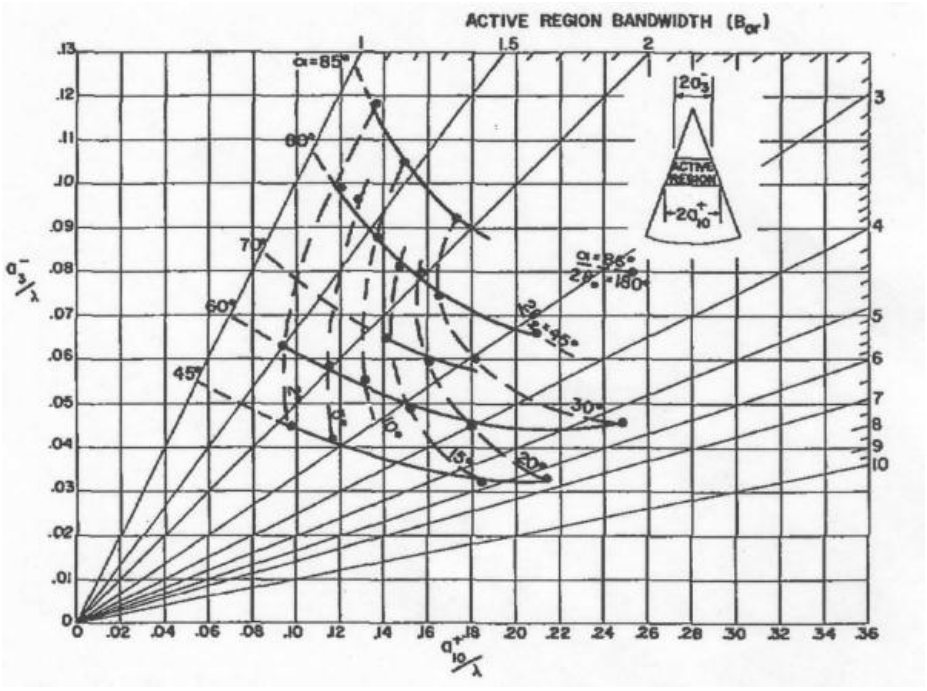

Figure 3.2 Active region constants with respect to wavelength of the CLSA [13].

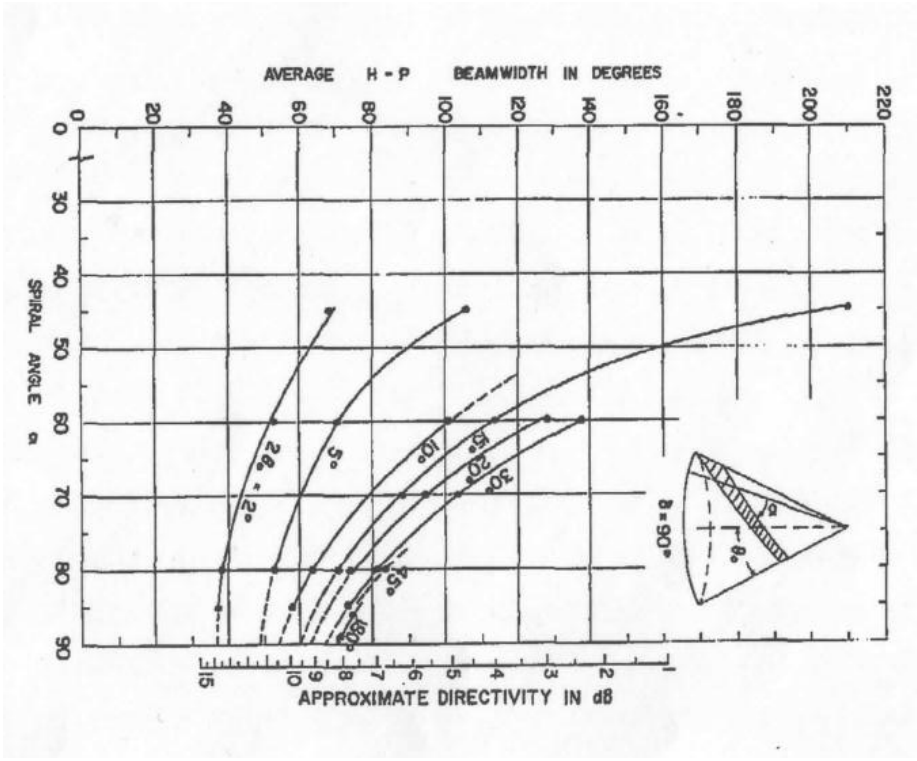

Figure 3.3 Average HPBW and directivity with respect to spiral and conical angle [13].

The directivity, as seen in Figure 3.3, is a function of the HPBW. The relation is such that as the beam gets smaller the directivity increases. Directivity, as discussed, is a measure of how an antenna directs energy with respect to an isotropic radiator. Thus with the decrease in main lobe beam width, the energy in the main beam must increase to compensate for the reduced beam angle. The connection between the antenna parameters is clear within Figure 3.3. As the conical angle and spiral wrap decrease and increase, respectively, the directivity of the antenna is increased. To satisfy the given requirements, the range of conical angles would need to be in the range of 60° to 80°. With these conical angles the spiral wrap would then need to be from 10° to 30°. The ranges give an approximate directivity of 6dBi, which is not accounting for losses within the antenna that constitute the gain measurement. Antenna efficiency and thus gain is simulated and given in Chapter 4.

Other aspects of the antenna that are directly related to the active region are the axial ratio. Figure 3.4 gives an example of the axial ratio for a constructed conical log-spiral of $2\theta_0 = 20°$. The minimal axial ratio comes from the direct center of the main beam, located at 0°, when the active region supports a main beam mode. Rotating away from the main beam, the axial ratio increases, where the spiral wrap determines the 3dB beam width. Larger values of the spiral wrap give an increase in directivity and decrease in HPBW, which would indicate that the main beam characteristically has a beam width of lower axial ratio values. Since the main beam is where the backfire radiation is emanating from, the axial ratio is directly correlated with the HPBW. As seen in Figure 3.4, $\alpha = 80°$ has a smaller axial ratio beam and increases more than $\alpha = 70°$ version. This is due to the decrease in the HPBW for $\alpha = 80°$ and thus the axial ratio follows the higher directivity in a smaller beam width.

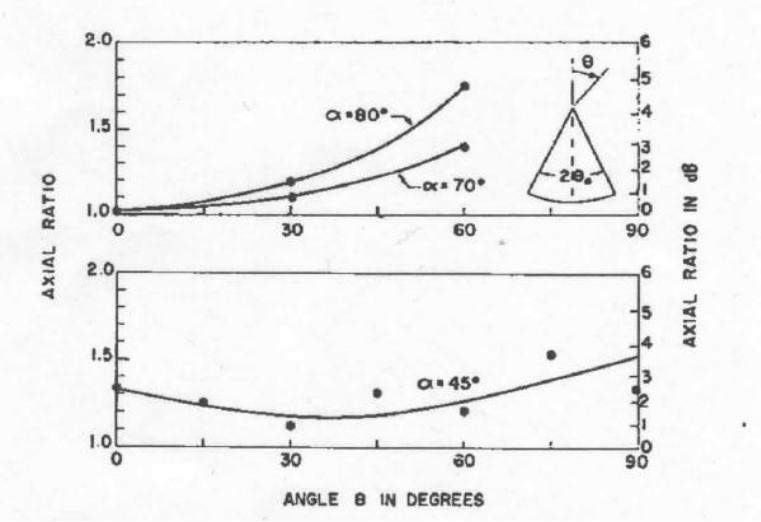

Figure 3.4 Typical axial ratio of the CLSA [13].

3.6 Preliminary Design

Relating all of the measured values to a meaningful format for design can be done by placing the design constraints to the respective beam characteristics. Table 3-1 and

Table **3-2** have been created from Dyson's measured data as design parameters and a starting point for creating an antenna and building in the domain of the simulation software package. There exist two possible designs and are from the a_{15}^{+} and a_{10}^{+} radii that determine the drop in near -field strength along the arms of the log-spiral at the lowest frequency of interest. To provide a smaller design for CubeSat applications, it is beneficial to reduce the size of the antenna, and thus the a_{10}^{+} design will be employed.

Table 3-1 Active region coefficients for a_3^-/λ with respect to the conical angle and spiral wrap.

	Total Conical Angle, $2\theta_0$			
Spiral Wrap, α	10°	15°	20°	30°
60°	0.054	0.051	0.043	0.055
70°	0.069	0.065	0.060	0.056
80°	0.089	0.083	0.079	0.070

Table 3-2 Active region coefficients for a_{10}^+/λ with respect to the conical angle and spiral wrap.

	Total Conical Angle, $2\theta_0$			
Spiral Wrap, α	10°	15°	20°	30°
60°	0.133	0.146	0.157	0.243
70°	0.130	0.144	0.160	0.183
80°	0.132	0.151	0.157	0.163

Using these values within Table 1 and Table 2, the upper and lower radius can be found based on the frequency band. This is accomplished due to the fact that the values are in terms of wavelength and only the multiplication of the upper and lower frequency bands is required. Choosing the value for θ_0=15° and approximating α = 75° from Dyson's data yield an upper and lower radius of:

$$a_3^- = 0.067\lambda_u = \frac{0.069c}{f_u} = 0.0528\ m\ (2.07\ in) = r_u$$

$$a_{10}^{+} = 0.172\lambda_L = \frac{0.124c}{f_L} = 0.214\ m\ (8.42\ in) = r_L$$

Thus these values give the conical parameters for the spiral arms that are provided by the designed equations. From the chosen conical angle and spiral wrap, the HPBW should be 85° with directivity of approximately 6.5dBi. These choices satisfy the given antenna requirements with the exception of input RL. By simulating the design presented in this section, the input RL can be confirmed and optimized depending on the input impedance.

The above equations describe the antenna truncation regions that are based on the same conical structure, with a frequency dependence modification that relates to the upper and lower radii. Extending the conical structure to infinitesimally small and large, with respect to the upper and lower radii, all frequencies are represented and any chosen upper and lower frequency is simply a slice out of the infinite conical construction. With this in mind, the only aspect that must be defined, within a fixed conical angle and spiral wrap, is the frequency band of interest. Therefore the next step is to create such a model to support the theoretical and measured analysis presented in this section for possible deployment on the CubeSat assembly.

CHAPTER 4

Conical Log-Spiral Simulation

To design and optimize the conical log-spiral with respect to the CubeSat application, the antenna is to be constructed within CST: Microwave Studio. The software is a simulation suite described as a "fully featured software package for electromagnetic analysis and design in the high frequency range" [20]. CST has many suites available for other applications, however for this thesis and brevity CST will be used to describe their Microwave Studio simulation domain. The suite offers various types of electromagnetic solvers, most of which are used when advantageous to operate one method over another. One of these aspects is the frequency bandwidth, where with conventional frequency domain solvers the software solves the system at each frequency point defined. This method requires significant memory overhead and may place the simulation in a computationally intensive environment. Fortunately the CST simulation suite

also offers time domain simulations that are not heavily affected by size of the frequency band, as the accuracy of the simulation is determined by the cell meshing. Specifically the cell meshing is given as the number of lines per wavelength, where 10 is the lower bound for accuracy in simulation [22]. For higher accuracy, the lines per wavelength can be increased at the cost of simulation speed.

This chapter will focus on the construction of the conical log-spiral within the CST simulation domain and the results from the constructed antenna. A detailed analysis of the antenna's construction will be provided, as many aspects of the construction were custom to the antenna. These results will be compared with the theoretical and measured results from Dyson's experimentation [13]. With the possibility of parameterizing the antenna design within the simulation software, the variables in design can be easily modified to find optimized values or completely change the design to offer different performance. Therefore, parameter sweeps will be performed to optimize the design and locate areas that can be improved. Lastly, one face of the CubeSat will be introduced to observe any significant changes to the radiation pattern. Conclusions on feeding mechanisms based on the simulated results will also be given.

4.1 Mapping CLSA Equations in CST

The equations for the conical log-spiral were given as a form of the planar spiral with the magnitude vector tracing the spiral arms as a function of increasing azimuth angle. This would give the smallest part of the antenna at the origin and can be manipulated to give a clear perspective of the antenna. It would be fortunate that the simulation domain would have a system for spherical coordinates; however this is not the case. Therefore the equations given in

Chapter 3 must be re-derived for the convention given in CST. The form for analytical face that needs to represent the CLSA governing equations follows the form of:

$$X(u,v); \quad Y(u,v); \quad Z(u,v)$$

Where, u and v are the parametric variables that are mapped to the function of the conical log-spiral. Since there is no increasing φ value, the increase of *u* and *v* have a requisite of tracking a similar function. Focusing on the initial curve, which predominately represents a line, the *u* variable must be within a function that mimics an increasing and yet rotating curve of the equiangular spiral.

To find the starting values for all x-, y- and, z-coordinates the cross-section of the conical structure is given in Figure 4.1. The non-shaded region is the cone that will be used to confirm that the resulting equations are correct for the antenna. The starting point in $X(u,v)$ and $Y(u,v)$ is the same as the upper radius and is expressed in terms of the defined cone as:

$$r_u = \rho_0 \sin(\theta_0)$$

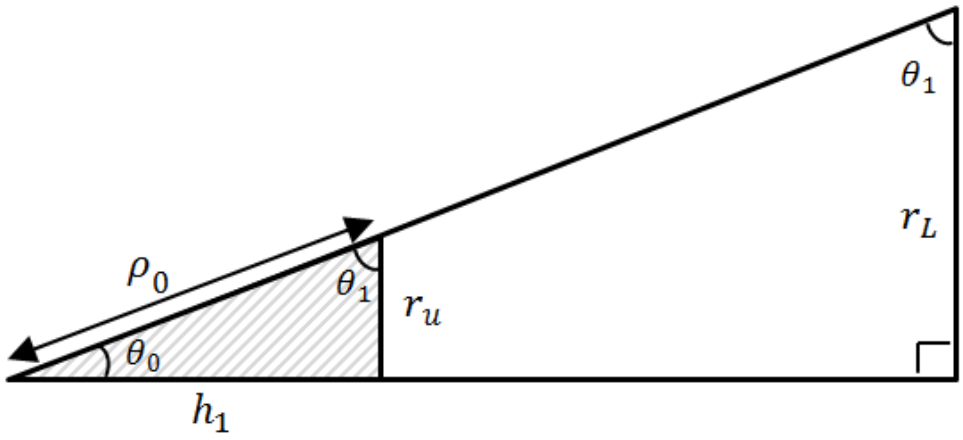

Figure 4.1 Geometry of the conical structure. Note that the shaded area is not a portion of the antenna.

Taking the equiangular equation to the parametric equation in CST is by the polar to Cartesian transformation. This implies that the x- and y-coordinate of the parametric equations are multiplied by cosine and sine, respectively. Giving that *u* will form the variable for the trace of the spiral and *v* will be the variation in width of the planar wire, $X(u,v)$ and $Y(u,v)$ are represented as:

$$X(u,v) = \rho_0 \sin(\theta_0)\, e^{\beta u} e^{\beta v} \cos(u) = r_u e^{\beta u} e^{\beta v} \cos(u)$$

$$Y(u,v) = \rho_0 \sin(\theta_0)\, e^{\beta u} e^{\beta v} \sin(u) = r_u e^{\beta u} e^{\beta v} \sin(u)$$

Each *u* and *v* component determines separate aspects of the spiral. If variable *v* was fixed the spiral would be a line trace of the equiangular spiral on a cone. Variable *v* introduces the variation of the wire such that it increases at the same rate as the radially outward spiral. The variable also introduces the conical angle to the planar wire such that it sits tangent to the surface of the defined cone. The starting point for the z-coordinate parametric equation, $Z(u,v)$, is based on the angle θ_1, which is defined as the complement of θ_0 (ie. $\theta_1 = 90° - \theta_0$). Following in a similar fashion, the starting point for $Z(u,v)$ is expressed as:

$$h_1 = \rho_0 \sin(\theta_1)$$

Thus $Z(u,v)$ is represented in a similar fashion to $X(u,v)$ and $Y(u,v)$, but does not need a trigonometric function that is only implicative to the x- and y-coordinates for the transformation from polar. $Z(u,v)$ is therefore represented as:

$$Z(u,v) = \rho_0 \sin(\theta_1)\, e^{\beta u} e^{\beta v} = h_1 e^{\beta u} e^{\beta v}$$

The range of *v* is the width of the wire, which is arbitrarily chosen to not interfere with the cone by being too large and not give high input impedance by being too small. The range *u* is

determined by the smallest value needed, or the starting point, and the maximum point of the spiral arm where the radius of the cone is r_L. This is found by setting:

$$X(u_{max}, 0) \cong r_L = \rho_0 \sin(\theta_0)\, e^{\beta u}; \quad u_{max} \cong \ln\left(\frac{r_L}{r_u}\right)(\beta)^{-1}$$

Therefore the range of values for *u* and *v* are:

$$u\colon [0, u_{max}]; \quad v\colon [-width, 0]$$

The derived equations for the parametric form are to be used in the simulation domain to construct an analytical face. This represents a planar structure that is not yet ready for the time domain solver. Other aspects must be refined to achieve the correct performance from the simulated antenna. The next step would be to confirm the antenna dimensions with the derived equations and define the port with which the antenna will be excited.

4.2 Spiral Arms and Feed Construction

Using the parametric equations defined in the previous section, the spiral arms are created using the analytical face equation editor. Since the single set of equations only represents one arm of the antenna, the second arm is created by using the exact formula with a 180° rotation introduced into the cosine and sine term of $X(u, v)$ and $Y(u, v)$, respectively. Figure 4.2 is the two arm log-spiral on the cone defined by the upper and lower radius of the active regions. Within the time domain simulator, the spiral arms must be resolved in the cell meshing and thus must be given a thickness. The thickness is a meshing issue and aspects of this facet will be discussed further in the following section after full construction and parameterization of the antenna.

With the planar spiral arms produced with the analytical face function in CST, the planar arms are given a thickness by activating the thicken sheet function in CST. The function protrudes the face along the surface of the spiral arms to the given thickness. Truncating the top and bottom portions of the spiral arms is the next procedure. To perform this process cylinders are constructed above and below the arms and a Boolean subtract operation is completed to remove excess parts of the spiral arms.

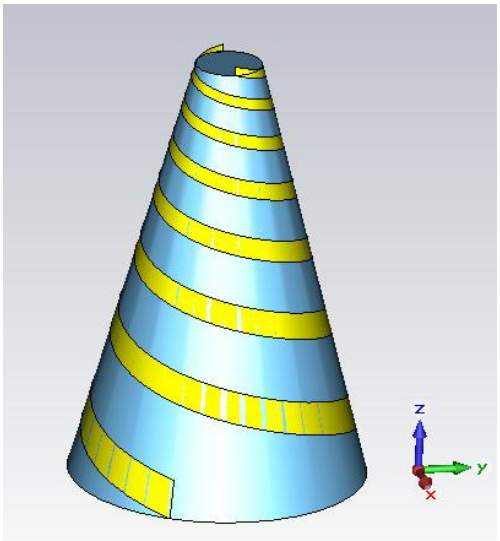

Figure 4.2 Initial spiral arms constructed in CST.

The feeding structure will be a discrete port across the top of the cone to each of the spiral arms. A custom structure for feeding purposes is built such that it would reduce the distance the port would cover across the top of the cone, as this distance will affect the port definition along the meshing axis. To prevent further port distortions that can lead to a failing port definition, the antenna structure is rotated by the z-axis to line up with the x-axis in the simulation domain. This means that the port will not be discretized between two or more mesh

cells; rather it will be represented as a line along one mesh cell plane. Extending a layer from the top of the spiral arms inward from both sides, the feeding structure is completed. The discrete port is now setup across the feed gap being located at the center of the wire. The thickened spiral arms, custom feed, and discrete port can be seen in Figure 4.3.

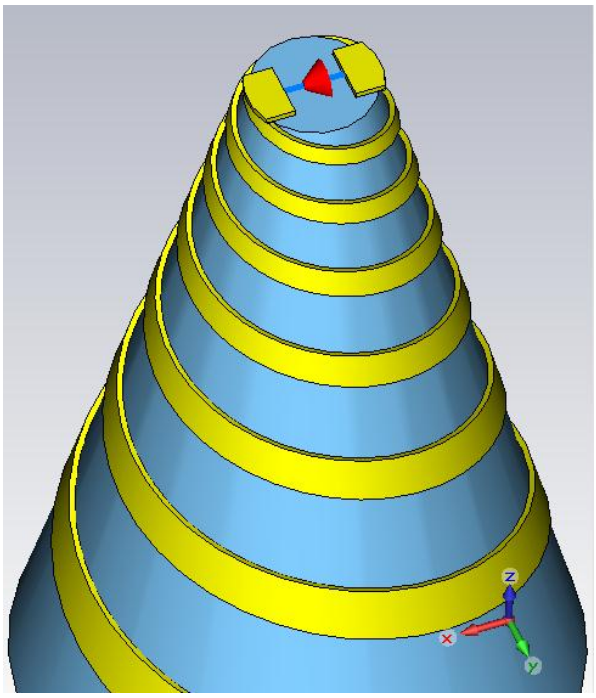

Figure 4.3 Extended layering of the spiral arms with custom feed discrete port.

4.3 Custom Cell Meshing and Simulation Accuracy

One aspect that must be carefully controlled is the minimum cells step, as this determines the minimal stable time step at which the simulation can run without encountering unstable wave propagation. The mesh must be refined on certain objects to resolve them in the simulation domain. Without proper resolution, the simulation will not accurately portray the electromagnetic structure and will give incorrect results. These aspects will be addressed

however the prevalent equations for the time domain simulations will not be presented but referenced for conciseness.

The thickness of the wire used in the simulation is 0.5cm, but this should not play a significant role as the radiation characteristics of the antenna are based on the active region where the current is flowing along the wire. Current flows mostly on the surface of the metal, with the exception of the skin depth. Since the material is copper, the skin depth is relatively small [18]. Therefore when the thickness is resolved, the aspects to play a role are the current on the surface and the defining waveguide structure of the spiral arms. For the global simulation the number of lines per wavelength resolution of the spiral arms was chosen to be 15, representing a slightly higher accuracy than the minimal 10 lines per wavelength [22]. Investigating the resolution of the mesh about the spiral arms, it can be seen that there is approximately one cell at the smallest component. At the upper part of the spiral arms the structure is not resolved, as seen in Figure 4.4. Refining the mesh globally will result in all of the cells being a single mesh step and thus an increase in the total number of mesh cells. Avoiding the overall increase in mesh cells is done by choosing the spiral structure and defining mesh that will resolve the thickness chosen. A larger thickness could have an adverse effect on the simulation, due to the increase of the active region. Minimizing the error of the active region is important to the accuracy, but it does have the tradeoff of longer simulation times. The resolution of the mesh cells for the chosen wire thickness was approximately three, two cells to resolve the inner and outer conductor and one to act as a place holder for the conducting spiral structure. The reduction of the mesh can be completed in the x-, y-, or z-direction, which limits the reduction to the selected component within the simulation domain. A comparison of the mesh in the cross-section wire of the initial 15 lines per wavelength and spiral refined mesh is found in Figure 4.4. Not only do

the spiral arms need mesh refinement, the port structure is in need of a smaller mesh step. By selecting the appropriate feed components, the mesh can be reduced in the Cartesian directions needed.

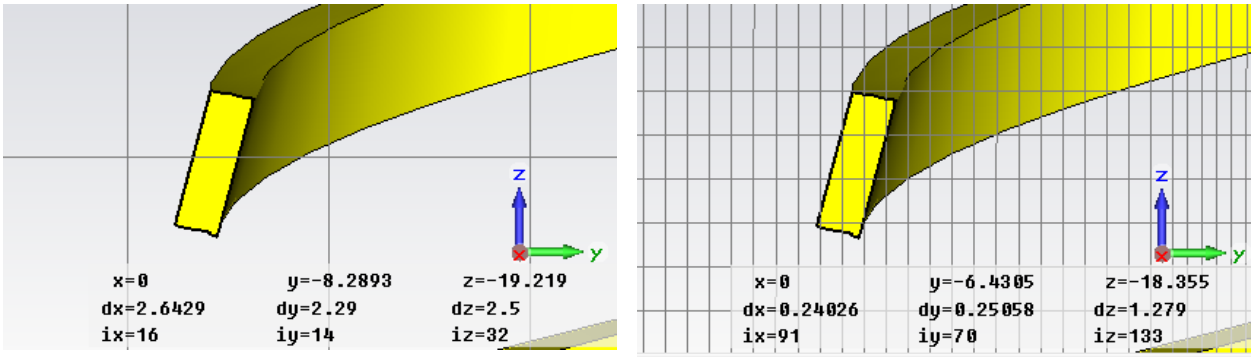

Figure 4.4 Refinement of the cell meshing. Initial mesh (left) and refined mesh (right).

With the mesh accurately representing the conical log-spiral, the time domain simulation can be initialized. CST offers a mesh refinement tool that provides several simulations with consecutive reductions of the mesh to calculate the convergence of the S-parameters. This aspect will be performed manually due to the nature of the custom and optimized meshing of the log-spiral. One other accuracy concern for the time domain simulation is the dissipation of energy after the excitation waveform has been introduced. The time domain can be terminated when the energy left within the simulation domain is below a certain level, typically -30dB. Energy is thus injected into the simulation domain through the port and the remaining energy is reflected back, dissipated, or radiated. The amount of energy left in the simulation after termination is bound by a truncation error, where the lower the defined energy level the less amount of error will be present.

4.4 Simulated Results

The results without optimizations obtained from the simulation are presented in this section. Results that will be focused on are the input impedance, radiation patterns, and circular polarization. The main objective is to see if the results are constrained by the required parameters and if the theoretical analysis forms a valid comparison. The theoretical value for a planar spiral is 60π (188Ω), however from experimental results the impedance can vary with the width of the spiral arms. A lower value of 150Ω is chosen for the input impedance and can be modified if needed. The accuracy of the simulation was set to a -40dB.

The simulated gain will also be presented within this section. The gain is addressed within the simulation due to the fact that the modeling was completed with lossy materials and the gain is an aspect of the computational domain. The radiation efficiency across the bandwidth of operation is investigated to determine if there is a significant difference between directivity and gain. Dyson measured experimental antennas in terms of directivity; however this incongruence is consistent with the time frame that the IEEE standard for gain was derived [18].

4.4.1 Input Return Loss

The simulated return loss is shown in Figure 4.5. With a return loss of -10 being the target, finding the best value for the input impedance is found by setting a parameter sweep of the defined port impedance. Several values will be simulated, showing trends within the S-parameter S11 of the increased impedance. Since the input impedance is the only parameter value that does not quite satisfy the antenna requirements, an optimization of the input

impedance for the antenna is completed. From the data it can be seen that the input match is better at the increased values for the impedance, with an optimized range of 190Ω to 210Ω. The remaining simulations will utilize an input impedance of 210 Ω.

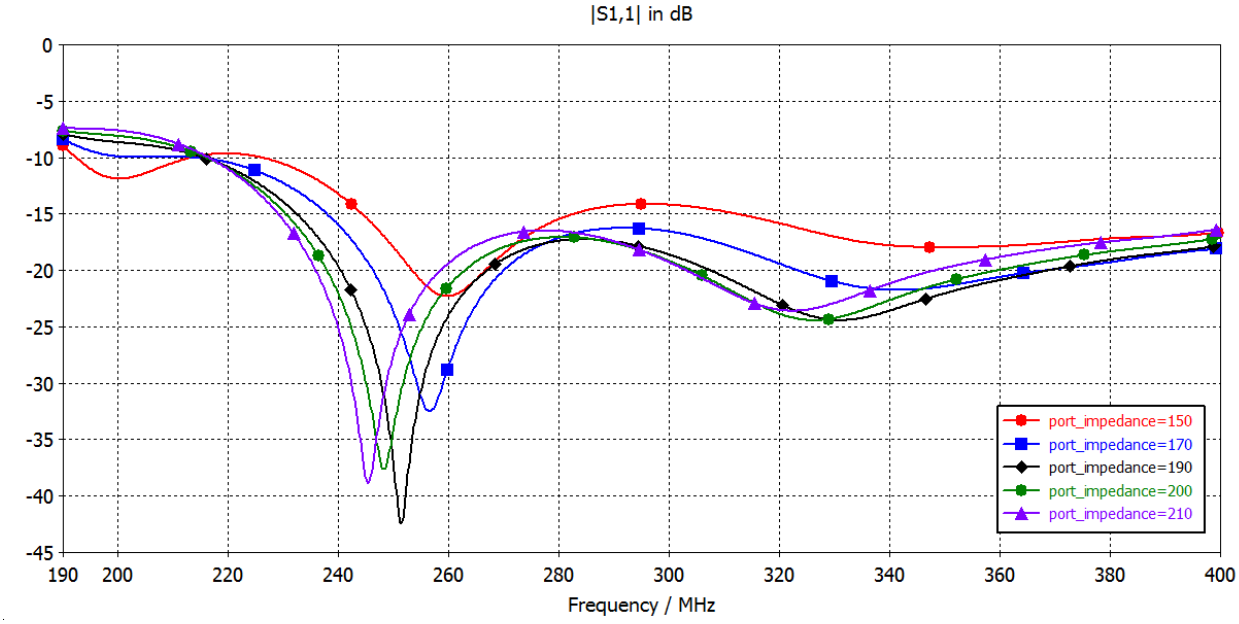

Figure 4.5 Sweeping port impedance for optimal input return loss.

4.4.2 Efficiency and Far-Field Radiation

Determining the radiation efficiency gives the gain of the antenna over that of an isotropic radiator. If the efficiency is large then the directivity is approximately the gain without the losses associated with the input match. Combining the input match and radiation efficiency is called total efficiency within CST. Both parameters are built into the simulation domain of CST when initializing material properties as lossy. By applying a loss tangent to the material components, the efficiency of the antenna as a radiator is calculated. Radiation and total efficiency of the CLSA is found in Figure 4.6. With the high efficiency results, the directivity is approximately equal to the gain of the antenna.

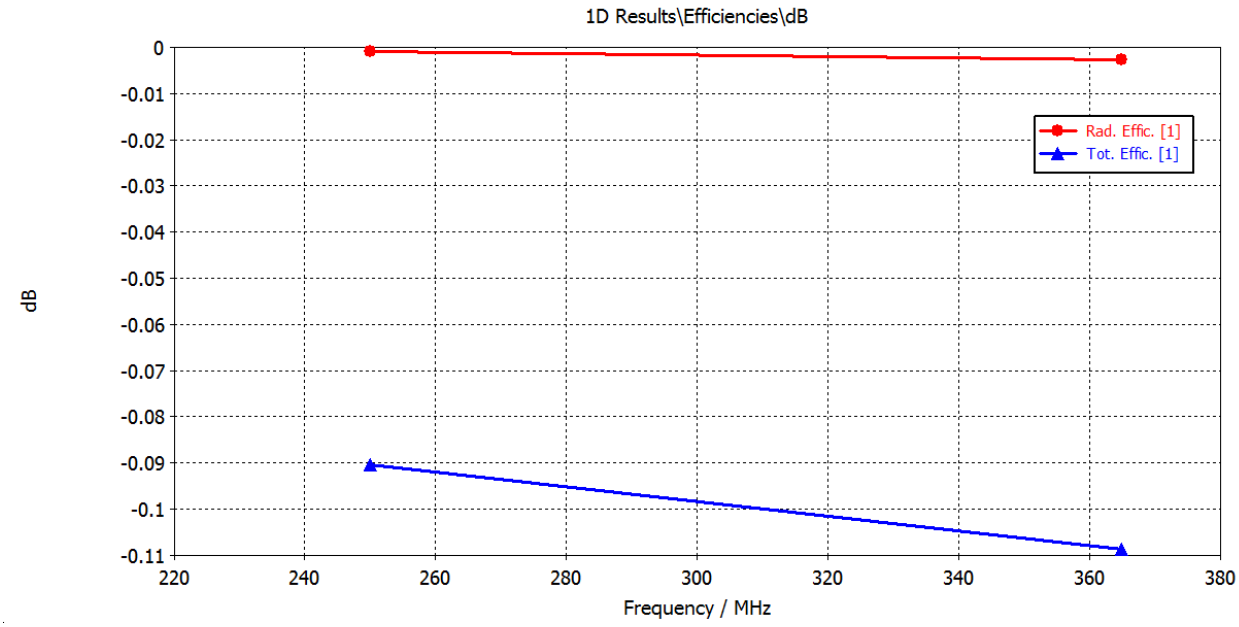

Figure 4.6 Radiation and total efficiency of the simulated CLSA.

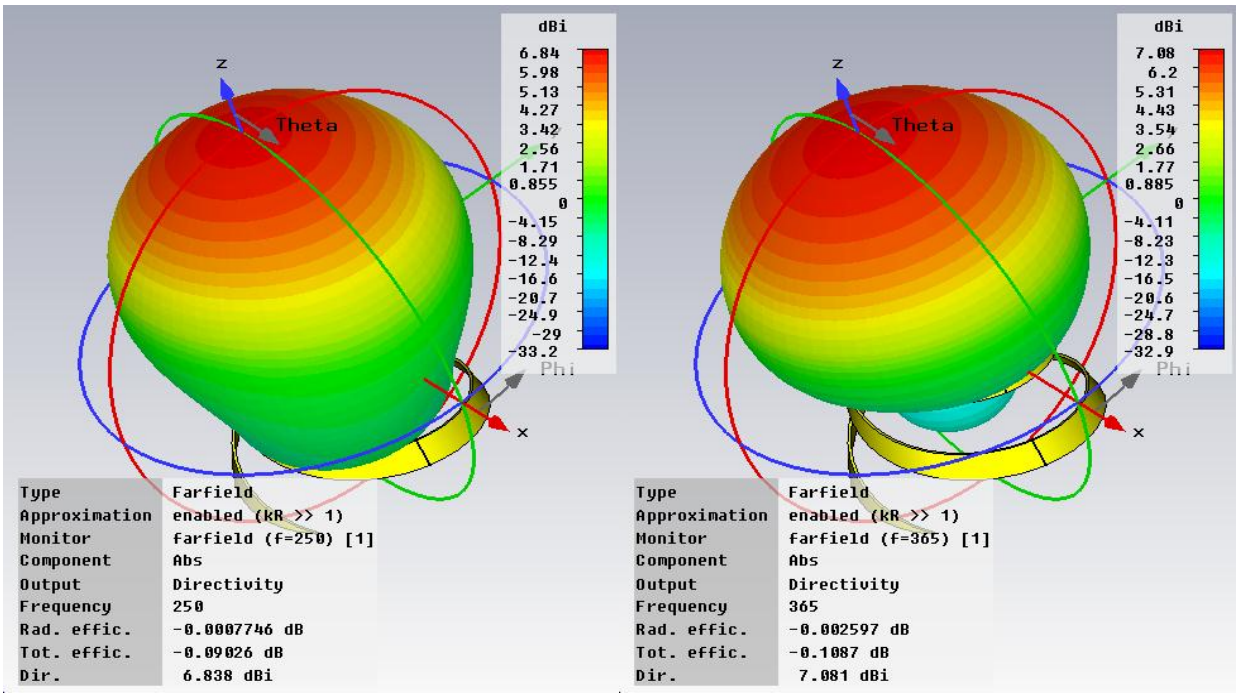

Figure 4.7 Far-field directivity at 250 MHz (left) and at 365 MHz (right).

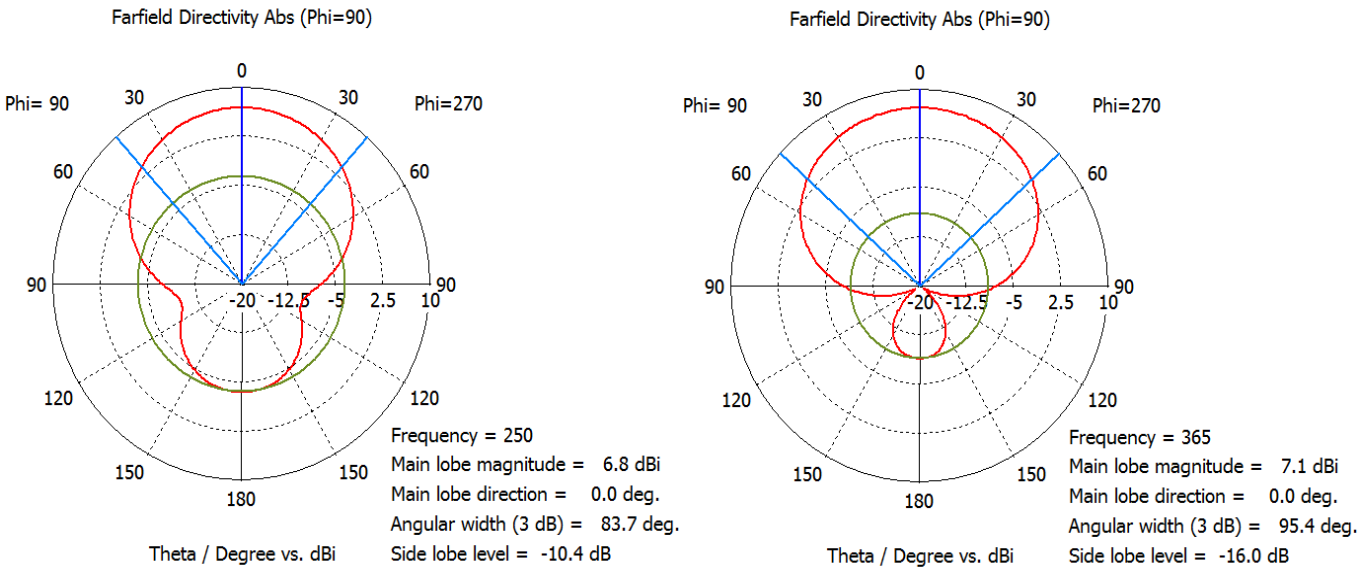

Figure 4.8 Polar cross-section of far-field directivity at 250 MHz (left) and at 365 MHz (right).

Far-field results when the characteristic port impedance is 210Ω at the upper and lower frequency bands is seen in the left and right hand side of Figure 4.7, respectively. Figure 4.8 shows the polar plot comparing the directivity at the band edges. Since the far-field patterns are not dependent along the φ angle, the polar plot is a good representation of the directivity in the constant φ plane with dependence on the θ angle. The 3D results are given for antenna reference with respect to the directivity, as the gain and directivity are approximately the same. Note that the radiation is toward the conical apex, as expected with the top feeding of the conical log spiral.

4.4.3 Axial Ratio

The next figure of merit is the axial ratio of the simulated antenna. Taking the optimized port impedance of 210Ω, the axial ratio of the upper and lower frequencies is shown in Figure 4.9.

The 3dB beam width of the axial ratio is double of that shown and is 132°, much larger than the HPBW. Having a larger beam that accepts circular polarization is beneficial. The main advantage is that the total HPBW does not suffer losses due to polarization and gives a guaranteed main beam where circular polarization is radiated.

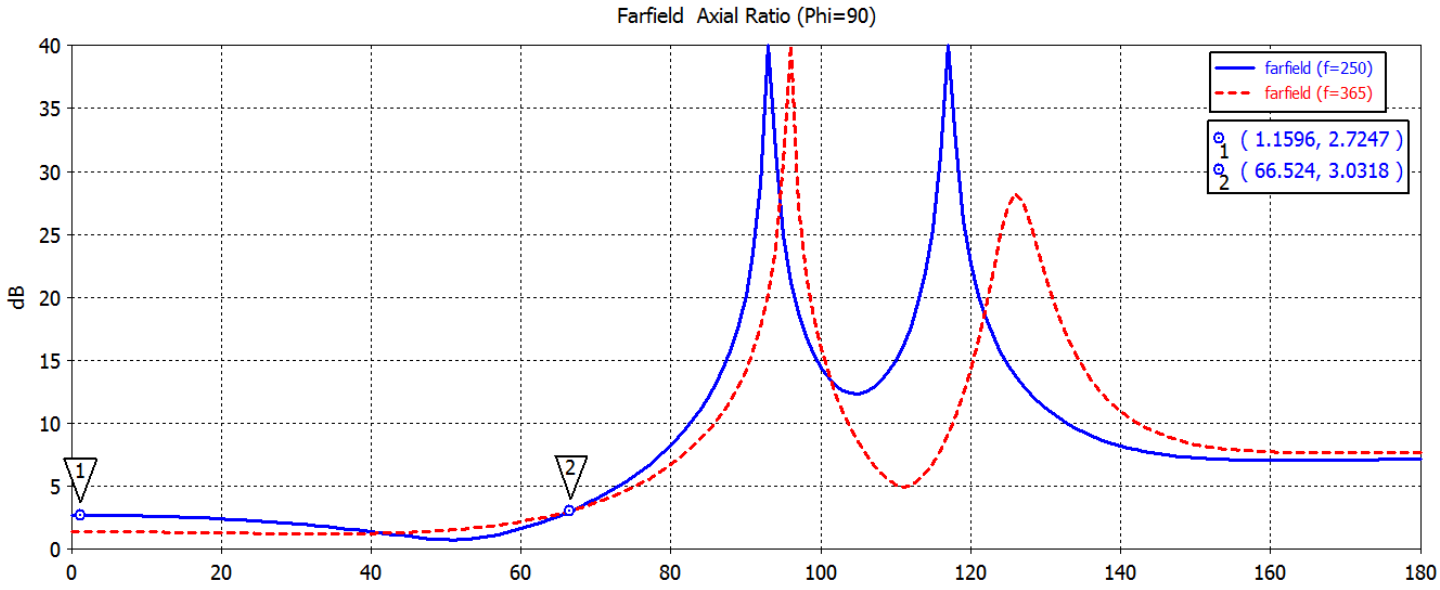

Figure 4.9 Cartesian Axial Ratio of the upper (365 MHz) and lower (250MHz) frequency.

4.4.4 Simulation Conclusions

There is a good agreement with the calculated parameters within Chapter 3 and the simulated results. The input match is below the -10dB mark across the frequency band, which means that at least 90% of the incident power is going into the antenna. The near unity radiated efficiency shows that the power on the antenna port is transmitted power. HPBW and directivity are calculated as 83.7° and 6.8dBi at the lower frequency and 95.4° and 7.1dBi at the upper frequency. As the frequency increases there exists a larger portion of the active region and the

guiding spirals, which explains the reduction in back lobe and the small increase in HPBW and directivity. Values within the simulation are slightly higher and lower, with the average value of HPBW at 80° and directivity of 7.5dBi, respectively. A minor deterioration in the axial ratio is seen in the lower frequency band, from choosing the a_{10}^{+} truncation to reduce the antenna size. Behavior at the lower frequencies of the band is not unexpected, as the drop in near-fields on the lower portion is only 10dB down from the maximum.

4.5 CubeSat Scenario

With the antenna giving similar results to the characteristics in Chapter 3, a scenario of introducing the three unit CubeSat will be investigated. By introducing the CubeSat as a perfect electrical conductor (PEC) "face", the effect of the additional metal on the radiated fields will be presented. Assuming that the antenna will face away from the satellite, with a flat portion under the antenna, Figure 4.10 shows the orientation and size difference of the antenna compared to the 30 cm x 10 cm CubeSat.

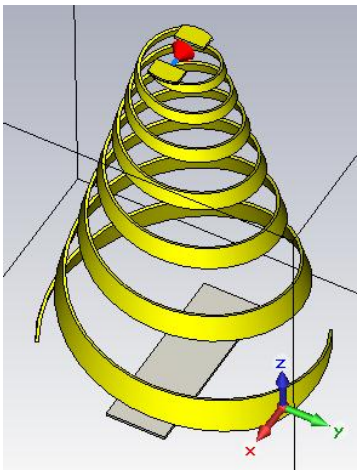

Figure 4.10 Orientation of the CLSA above the three unit CubeSat "face".

Effects on the radiated fields show little influence, as seen in Figure 4.11. The main differences are the slightly larger directivity at the upper band and the increase of the back lobe at 120°. One of the reasons for this slight change at the higher frequencies is the waveguide nature of the CLSA. At the upper band the backfire radiation is partially incident on the CubeSat "face" and gets scattered to form a back lobe as a result. The CubeSat "face" at the lower band is expected to have a greater impact, however this theory is incorrect. The back lobe radiation forms around the face with the PEC sheet having little effect. E- and H-fields were observed here to form results based on the field properties.

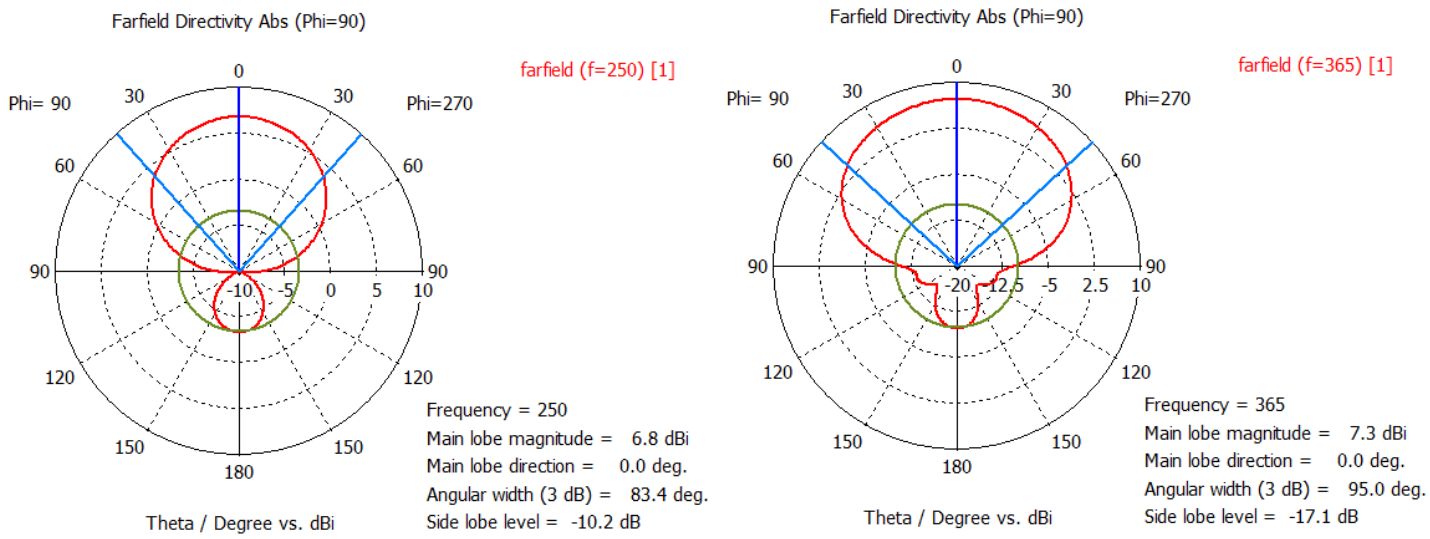

Figure 4.11 Polar cross-section of the CLSA with a CubeSat "face" underneath.

The frequency range needed from the requirements makes the size of conical log-spiral larger than the CubeSat, which was to be expected with the dimensions of the antenna given in

Chapter 3. Even with the size difference, it is possible to compress the antenna at launch and deploy it when the satellite is in orbit. One problem that arises out of the antenna presented is the feeding location at conical apex. The feeding would be coaxial along one spiral arm with a dummy coaxial located on the other spiral arm for symmetry [14]. This could lead to complications in deployment with the extra coaxial line attached to the already thin spiral arms, not mentioning how much weight this would add to the already payload limited CubeSat. Another method is sending a coaxial line to the top along the axis of the cone. Symmetry would be extremely important when placing a coaxial cable within the antenna's backfire producing area. The cable would need to be shielded to prevent any radiating back current from the feed and interference from the near-fields within the spiral arms. Minimal impact on radiated fields has been noted when the diameter of the shielding is less than one third the diameter on the top of the cone [13]. The type of shielding would be dependent on the near-field source being magnetic or electric [16]. With the field investigation yielding both as a source, shielding for both cases would need to be considered. Using this method of feeding would also be limited by deployment capabilities onboard the CubeSat, the main constraint being support structures for the antenna and shielded coaxial feed.

Noting the complications of the feeding scheme that deploying the CLSA would face, other methods should be studied and considered. The effects of changing the feed location have not been investigated by Dyson or any other researched author on log-spiral antennas. The best case for changing the feed location would be not to alter the antenna characteristics of the already designed log-spiral. Ideas and possible solutions to the challenging feeding techniques will be explored in the next chapter.

CHAPTER 5

Antenna Feeding for CubeSat Applications

Previously discussed in Chapter 4, the current feed of the CLSA poses deployment challenges due to the antenna size and feed location. Deployment would need to focus on the proper antenna characteristics and not the feed, since the active region defines all radiated characteristics for the antenna. Not having the feed location at the apex of the conical structure is essential to reducing the deployment structures. Therefore it is proposed that bottom feeding the CLSA designed in Chapter 4 be perused as a deployment option. This chapter focuses on the unique concept of bottom feeding for the CLSA, where results of simulated versions are given and analyzed.

5.1 Bottom Feed Investigation

Changing the location of the feed to the bottom of the antenna changes how the backfire radiation is produced. The active region should not be changed since the structure of the spiral arms have not changed. This means that the slow-wave nature changes into a fast-wave regardless of where the introduced antenna excitation is located. However, the active region described by Dyson was measured through the top feeding system and may change with a different feed location. Assuming that the wave changes directions and is backfired away from apex of the cone and toward the feed, the radiated fields would be directed towards the CubeSat. To compensate for the reversed direction of the backfire, a ground plane below the antenna is proposed to provide an image that redirects the radiation towards the conical vertex. This should result in patterns similar to that of the CLSA designed in Chapter 4. To provide evidence of the proposed feeding, simulations are given.

Using similar methods to simulate the antenna as in the previous chapter, the custom top feed is removed and a custom bottom feed is constructed. The feed gap is exactly the same as the top feed to provide consistency. Concerns about the size of the bottom feed have been noted, with possible impact on the lower frequency axial ratio or radiation pattern. These aspects will be addressed should the need arise. Figure 5.1 shows the confirmation of the direction of the radiation pattern, which is toward the feed and away from the conical vertex. Since the active region was not completely mapped though the bottom feed process, a slight deterioration of the radiated fields at the upper frequency is observed. As mentioned before, the possibility of the active region moving due to the feed change was a stated possibility. Before any modifications to the antenna are preformed, the effect of a ground plane is investigated. It has not been

discounted that the antenna could gain the performance it had with the placement of a ground plane.

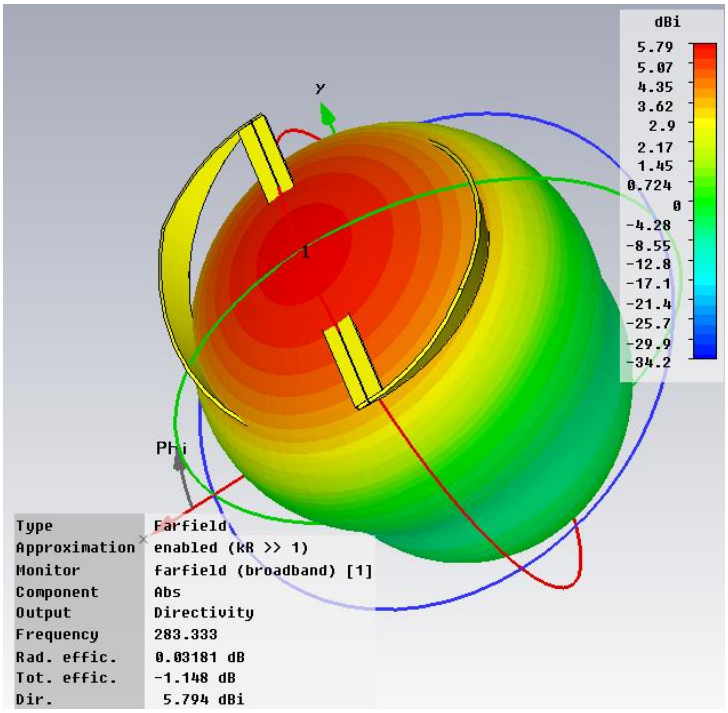

Figure 5.1 3D far-field directivity using proposed bottom feeding scheme.

5.2 CLSA Ground Plane

Confirming that the radiation does indeed get redirected, a ground plane is added to the antenna system for characteristics that are similar to the top feeding arrangement. Abiding the symmetry of the antenna, a circular ground plane was chosen. The following sections go through various degrees of freedom granted by the introduction of the ground plane.

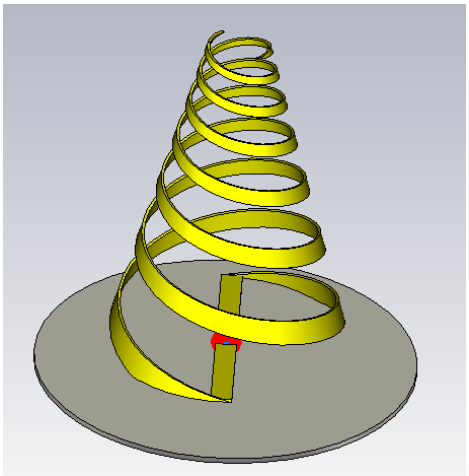

Figure 5.2 Placing a circular ground plane underneath the bottom fed CLSA.

5.2.1 Ground Plane Radius

The larger ground plane is better, as the antenna will reference ground anywhere it can find it. Giving the antenna a large ground plane will provide this reference, however it must be reduced for CubeSat applications and at the same time retain optimal antenna characteristics. Therefore the radius of the circular ground plane is simulated over several values.

Parameters being watched over in the simulation range are the input impedance and the far-field radiation. With the input impedance being unknown, it was chosen to be value of 210Ω. Increasing the ground plane radius has significant changes within the impedance bandwidth and radiated fields, as seen in Figure 5.3 and Figure 5.4, respectively. From the results of the parameter sweep, the radius that gives the best impedance bandwidth and radiated fields is a radius is 35cm (13.78 in). Other aspects that need to be considered are the impedance and height of the antenna above the ground plane.

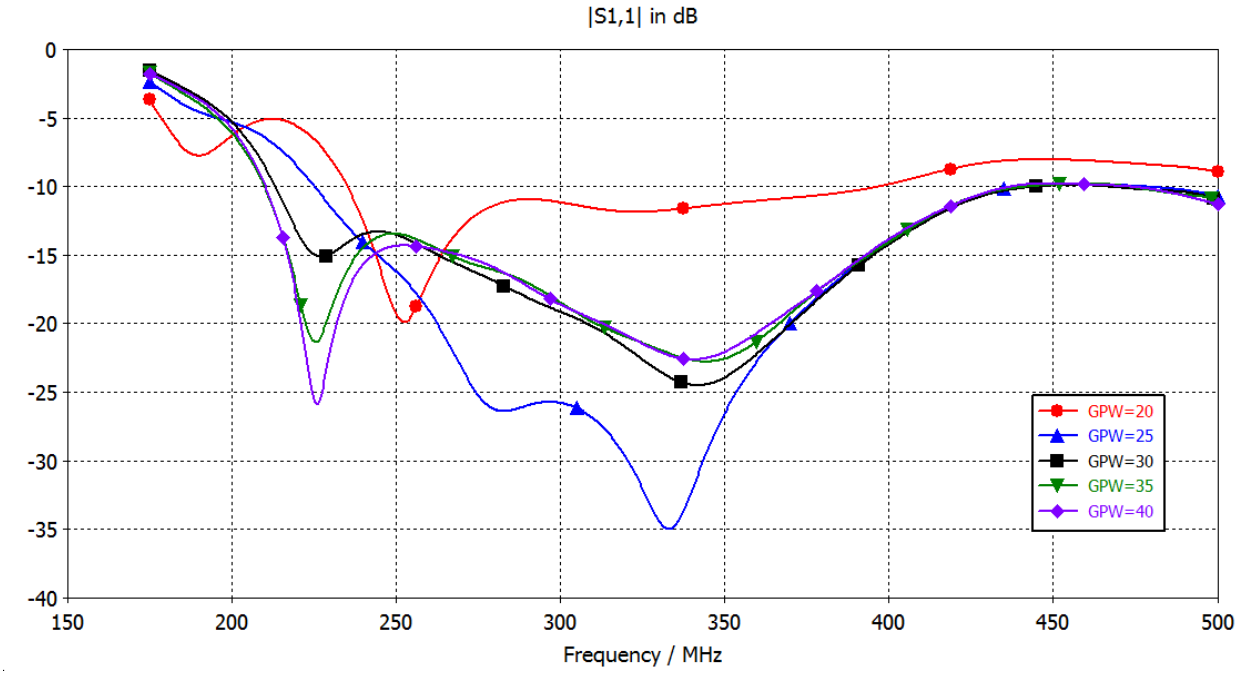

Figure 5.3 Input return loss through a sweep of the ground plane radius (seen as GPW).

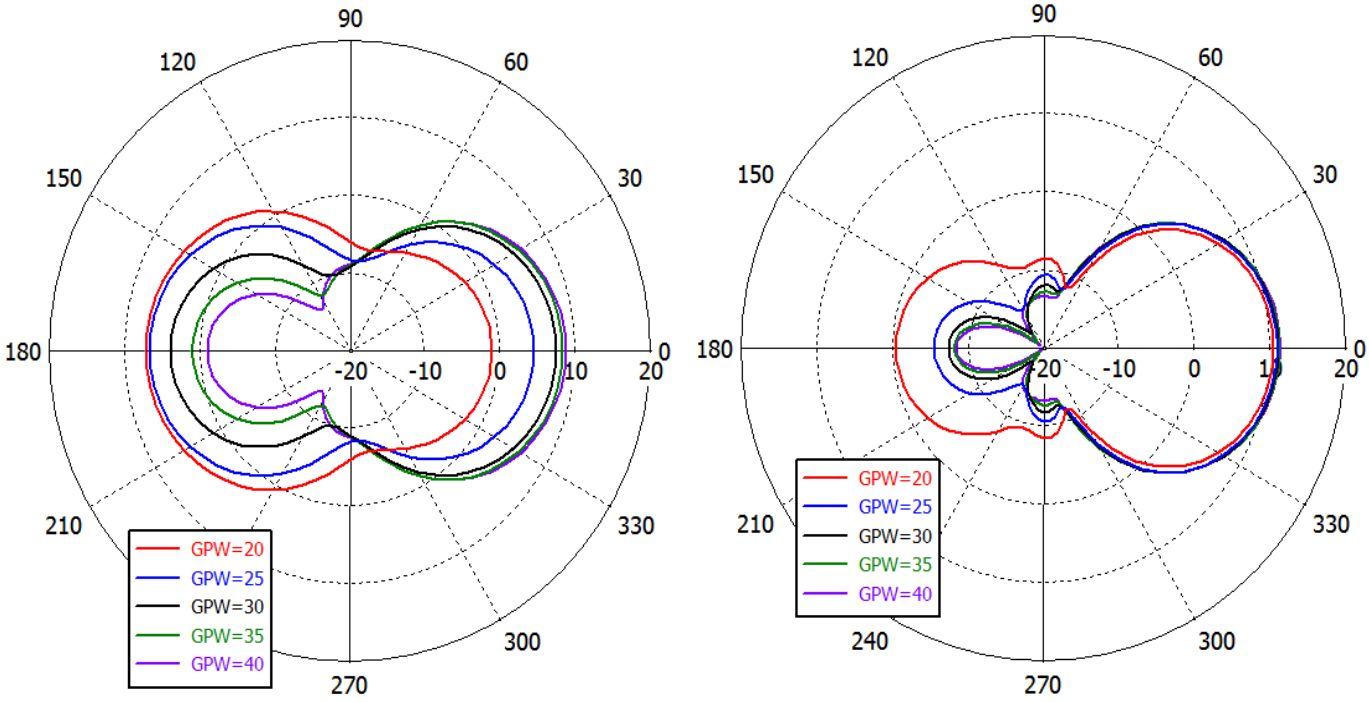

Figure 5.4 Polar cross-sections of the far-field directivity for increasing ground plane radius (seen as GPW). Note: zero on the polar plot is towards the conical vertex.

5.2.2 Height Above Ground Plane

During simulations, it was noted that changing the height of the antenna with respect to the ground plane had significant effects on the input RL. Simulating the antenna height above the ground plane is completed and the results are in Figure 5.5, where height is given in centimeters and the port impedance is 150Ω. As height is reduced, the input RL of the antenna is improved. Further reduction introduces capacitive loading on the feed and RL is thus increased due to input mismatch. RL can be improved with knowledge of the input impedance. With the top feeding CLSA, the impedance was higher than the 150Ω value. Explorations of port impedance are discussed within the next section.

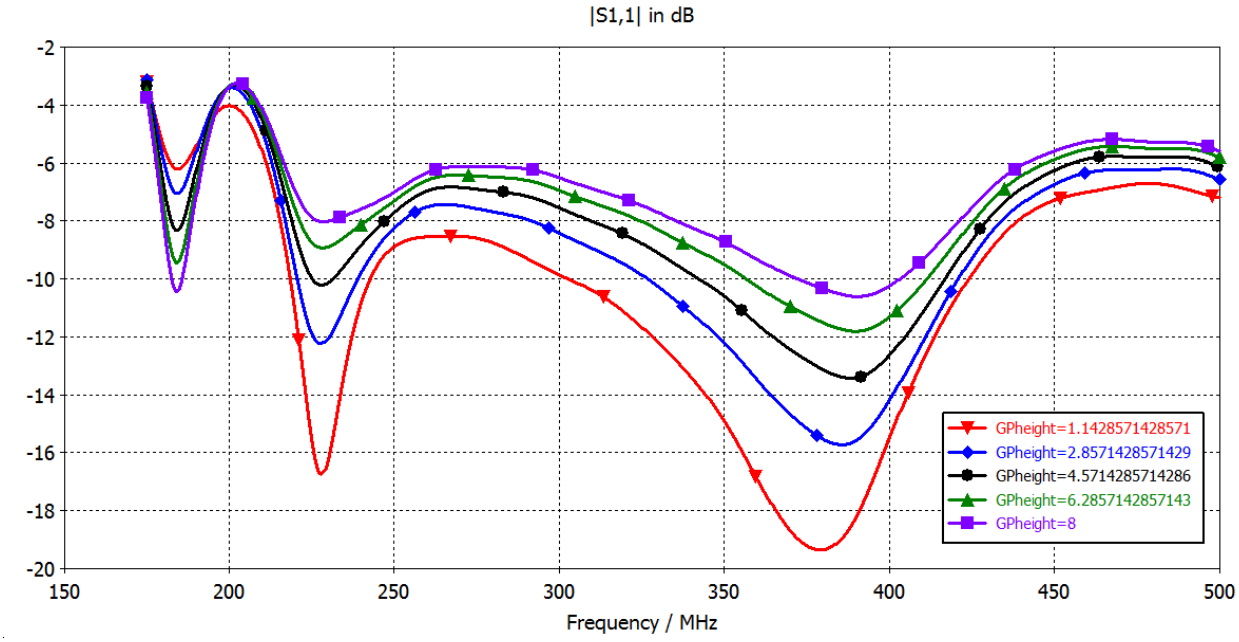

Figure 5.5 Return loss results when sweeping the height above the ground plane. Port impedance is 150Ω.

5.2.3 Input Impedance

The input impedance is not known for the bottom feeding configuration and could have changed from the value optimized within Chapter 4. Sweeping the impedance of the port, the resulting input RL is seen in Figure 5.6. The port impedance range that gives the required RL of -10dB is 190Ω to 210Ω. The range could be extended to include 170Ω since it has the lowest value for S11. However, the RL for 170Ω is close to the -10dB mark around 250MHz, which does not leave much room for error. The impedance of 210Ω has a larger bandwidth below the -10dB mark and leaves room for inaccuracy that inevitably is encountered with antenna construction.

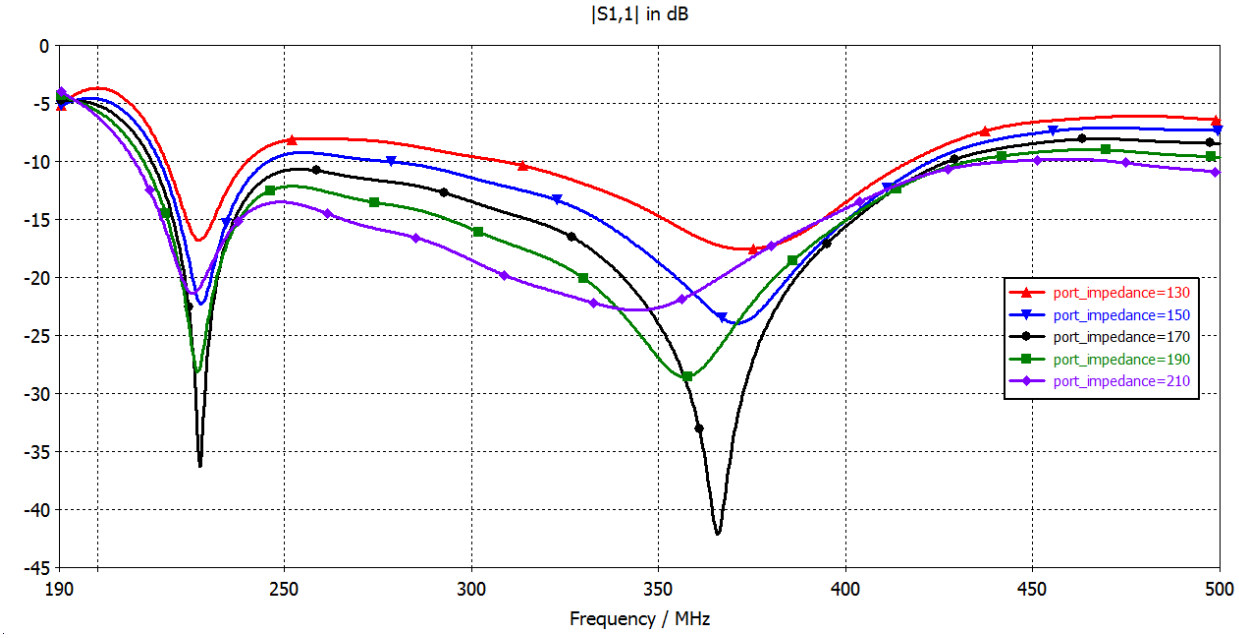

Figure 5.6 Return loss through a sweep of the port impedance.

5.3 Bottom Fed CLSA Conclusions

With all of the parameters rigorously simulated, the results are comparable with the top fed CLSA simulated in Chapter 4. A major difference is the increase in directivity as frequency increases. This is to be expected, as the ground plane is electrically larger at the higher frequencies. There is a slight deterioration of the axial ratio at the lower band edge. Suspect for this occurring is the feeding mechanism, being a large horizontal component that has the capability of disrupting the axial ratio calculation within the simulation. When observing the electric field, the rotation of the phase can be seen when looking at the antenna in the bore sight. For the bottom feed configuration, the higher frequency phase is seen rotating about the *z* axis. The lower frequencies, however, are rotating with a distortion that is aligned with the bottom feeding mechanism of the antenna. There is not a uniform phase rotation seen and this could be causing the distortion. Many attempts were performed to improve the lower band axial ratio, with no success. It is believed that the long feeding arms are disrupting the axial ratio within the simulation environment. The feeding structure is to be changed when antenna construction occurs, which includes the removal of the long feeding arms. Therefore, the deterioration of the axial ratio will be determined by measured results presented in Chapter 9.

CHAPTER 6

Frequency Scaling for Antenna Construction

To simplify the construction of the CLSA, it was decided to scale the design to a higher frequency. Scaling to a higher frequency will make the antenna smaller and thus fewer raw materials will be needed and the far-fields can be tested in a smaller space. This also provides an opportunity to test the robustness of the design over various frequency bands within the simulation domain. As discussed in Chapter 4, the parameters that would need to be change are the upper and lower frequency. This can easily be changed within the "parameter list" created in the CST. More on the CST modifications are discussed further in this chapter.

Before changing the frequency, it must be noted that a single frequency can be scaled straightforwardly. However a frequency band will not scale by a multiplication to an arbitrary

frequency. The proper process is to use the percent bandwidth with chosen band edges. As before the band edge form of percent bandwidth is defined as:

$$FBW = 2\frac{f_2 - f_1}{f_2 + f_1}$$

Since the FBW is known and f_1 is chosen, f_2 can be determined as:

$$f_2 = f_1\frac{(FBW + 2)}{(2 - FBW)}$$

The equation now gives the percentage bandwidth as a constant and the upper band edge and lower band edge as functions of each other. Therefore a FBW of 53% and a lower band edge of 2GHz yields:

$$f_2 = (2GHz)\frac{(0.53 + 2)}{(2 - 0.53)} = 3.44GHz$$

With the new band edges, the frequency band for the scaled conical log periodic antenna becomes 2GHz – 3.44GHz. With parameterization already completed in Chapter 4, the new band edges can be plugged directly into the simulation domain. Other factors will need slight adjustment and these include the planar wire thickness and width, since the relative size is much larger within the higher frequency bandwidth.

Determining an arbitrary lower band edge was performed by calculating the dimensions of the resulting antenna. The major goal of this was to give a design that would be easy to manufacture and fall within size tolerances. The tolerances given are based on the height of the antenna and the smallest width of the log-spiral arm. Theoretically the frequency independence of the log-spiral antenna can make the wire a small and unmanageable width for hand

construction of the antenna. The tolerances given are a wire width of 0.0254cm (10mil). Note that the widths of the upper spiral wire are estimates with relative scaled sizes to the port dimensions. This ensures that the antenna is properly scaled and will reproduce similar results to its UHF counterpart.

6.1 Modification to CLSA in CST

The modifications within CST are easily achieved due to the fact that the antenna was created with a list of parameters that are associated over the upper and lower frequency. The related parameters include finding the a_{10}^{+} and a_{3}^{-} values based on the active regions of the upper and lower frequency, respectively, for the chosen beam width. The beam width is also connected to the conical angle and the spiral wrap rate. These values were already determined in Chapter 3. To ensure that the antenna is working similar as the UHF design, the top feeding is implemented in the same fashion as before. The feed is a discrete port across the two arms of the log spiral with arbitrary impedance of 150Ω. From Dyson, this impedance is a typical choice for a number of conical log-spiral antennas and will be optimized once the correct response is observed and errors within the simulation are carefully considered.

The antenna is scaled within CST by changing the upper and lower frequency, which results in left hand side of Figure 6.1. The upper and lower radii are calculated to be 0.58 cm (0.23 in) and 2.57 cm (1.01 in), respectively. As the wire thickness was not considered to be a frequency dependent component, it did not change with respect to the new upper and lower band edges. Therefore, a new value of the thickness must be considered to mimic the results of the previously presented UHF log-spiral. Previously discussed within Chapter 4, the efficiency of

the simulation is based on the size of the smallest cell within the simulation domain. The resulting time step is thus much smaller due to the stability criterion of the time step with respect to the spatial step. The stability criterion for the time domain simulation relates to the thickness of the wire seen and will be reduced to adequately mimic the UHF design.

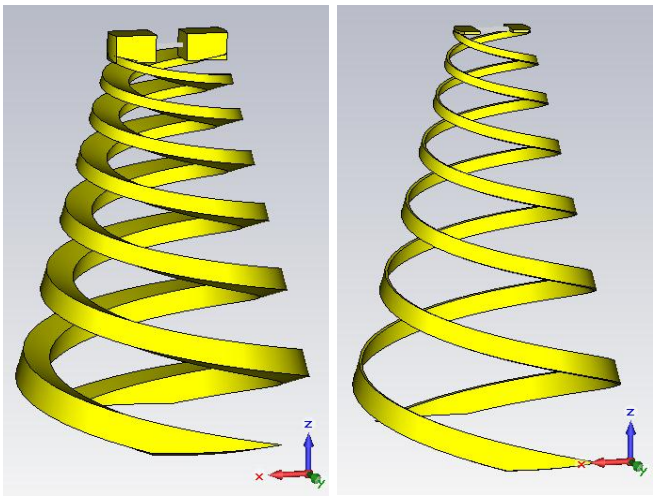

Figure 6.1 Comparison of unchanged (left) and scaled (right) wire width in the S-band CLSA design.

As the current will flow along the surface of the spiral arms, the thickness of the spiral arms will not play a major role. The case that this will not be true is when the thickness is interfering with the defined conical shape needed to define active regions for the frequency band of interest, as demonstrated in the left hand side of Figure 6.1. To form spiral-arms that do not interfere, the thickness and width of the wire was chosen to be 0.5 mm (19.68 mil) and 7 mm (275 mil), respectively. As before, the width is defined as the displacement of the bottom edge of the spiral arm from the given equiangular equation.

Checking the meshing about the spiral arms, the resolution of a bisected log-spiral arm toward the upper section of the conical section can be seen in Figure 6.2. The mesh around the

arms has been verified for this spacing, with at least three mesh cells occupying the z-, x-, and y-directions. It has been noted previously that the meshing can be within these thresholds and are proven by the convergence of the S-parameters. The mesh is within these constraints and can be revisited if the expected results are not obtained.

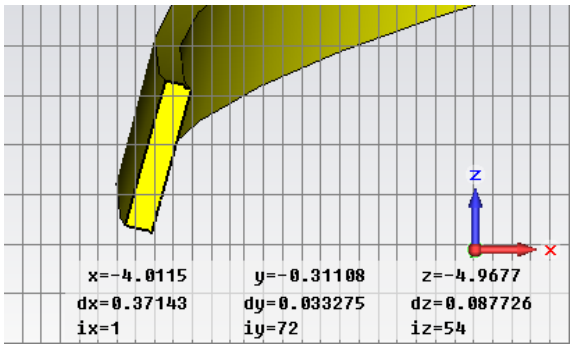

Figure 6.2 Cross-section of spiral arm to ensure proper cell resolution.

6.2 Simulation Results for S-Band Conical Log-Spiral

The CST simulator for the 2 – 3.44GHz conical log spiral is the transient solver, where the input wave form is a Gaussian envelope that contains the spectral excitation for the design frequency. With the ports already defined, the knowledge of port impedance is necessary. For the initial simulation the impedance was defined as 150Ω and will be optimized for the given structure. The transient solver was utilized at an accuracy of -40dB without the adaptive mesh refinement, as the mesh has been user defined and this may lead to longer than necessary simulation times for this structure. With the simulation domain carefully prepared, the initial results are presented in the following sections.

6.2.1 Input Return Loss

The S11, as the designation CST environment has assigned, is found within several steps of the port impedance in Figure 6.3, which was obtained from a parameter sweep in the simulation domain. From Figure 6.3, the port impedance with the lowest S11 magnitude is 210Ω. Rerunning the simulation at a higher accuracy yields almost an exact match to the S-parameter at 210Ω seen in Figure 6.3. With the convergence of the S-parameters seen, the accuracy of the model is verified and the other antenna characteristics should remain stable.

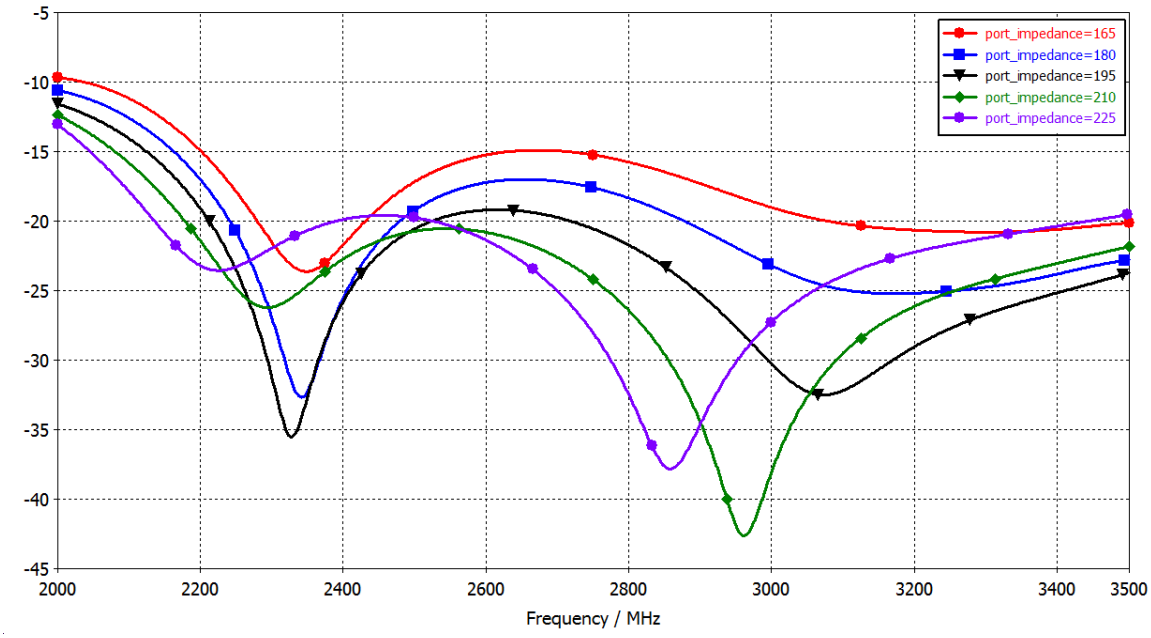

Figure 6.3 Return loss through a sweep of the antenna input impedance.

6.2.2 Far-Field Magnitude

The polar far-field result for the band edges is found in Figure 6.4. These plots are consistent with the UHF design of the CLSA presented in Chapter 4. Only a slight increase in the HPBW is seen in the upper frequency of the antenna.

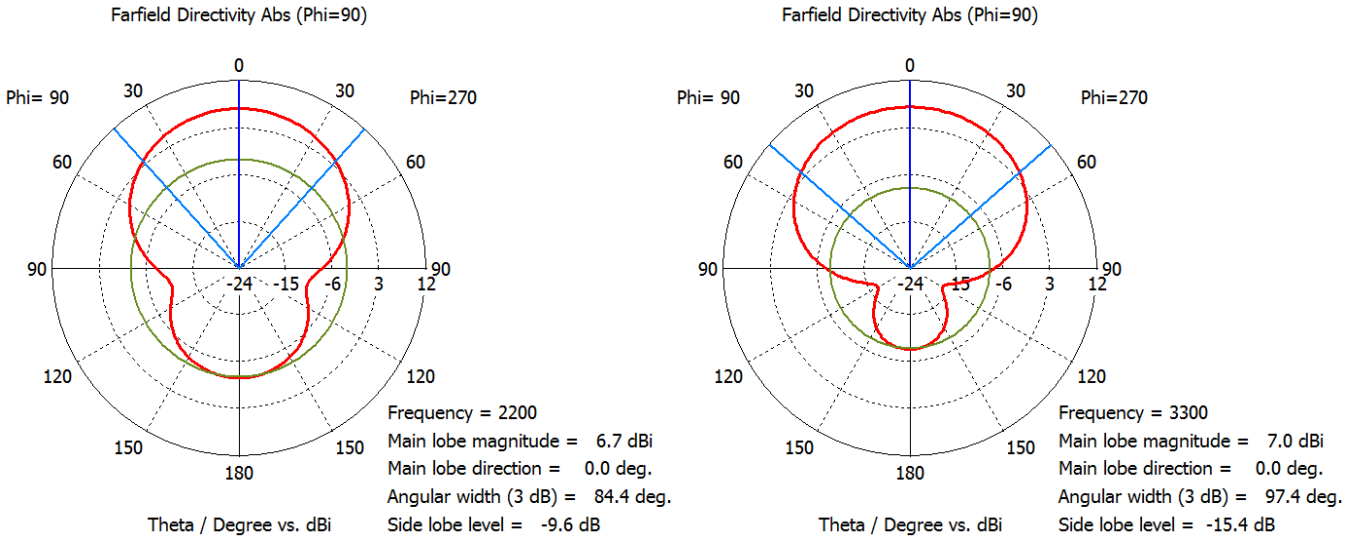

Figure 6.4 Polar cross-section of the far-field directivity at 2200MHz (left) and 3300MHz (right).

6.2.3 Axial Ratio

The axial ratio of the band edges are given in Figure 6.5. Points along the curve indicate that the axial ratio is below 3dB point for a half beam width of 68°. The total beam of the antenna that the AR is below 3dB is double of what is given, as this value only represents only half of the total beam.

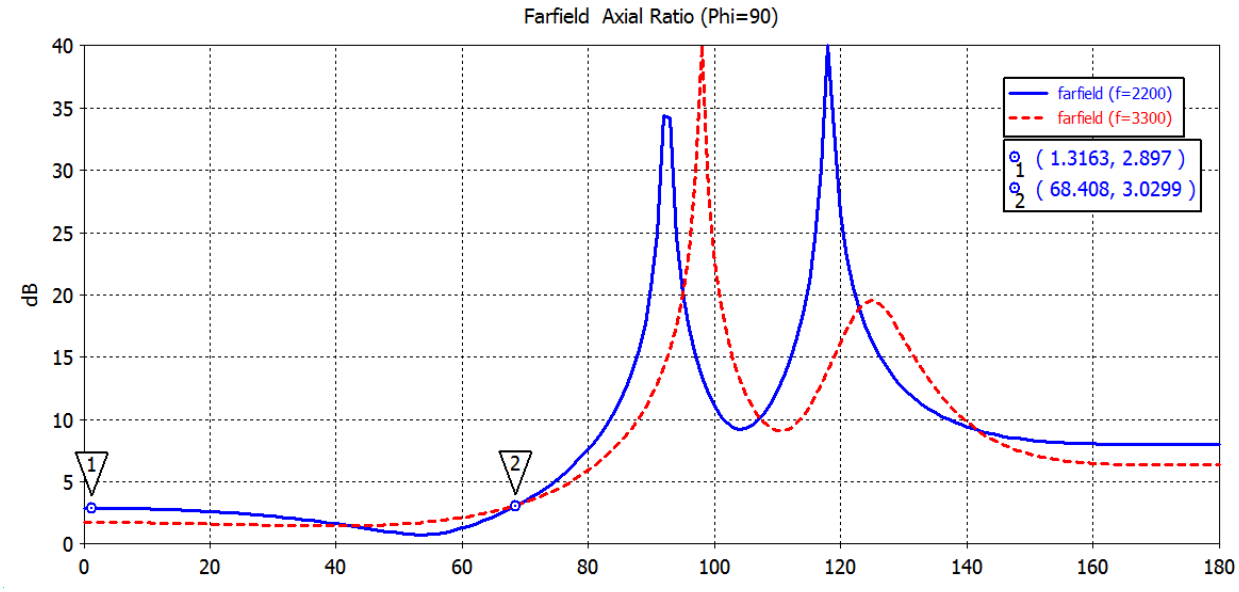

Figure 6.5 Cartesian plot of the axial ratio at antenna band edges. Note the beam width of the axial ratio.

6.2.4 Conclusions for S-Band Top Feeding

With the results of the simulation presented, it can be seen that the frequency shifted conical log-spiral holds similar results as its UHF counterpart. The axial ratio is almost an exact match and only a slight shift can be seen in the peaks. The beam width of the main lobe at the lower and upper frequency shifted slightly, but this can be explained by the variation of the far-field monitor in CST not located at the exact scaled frequency. The closeness of the results for the two designs are well within acceptable margins. With the scaled version, the design can be completed with the proposed bottom feeding technique to reduce the complexity associated with the deployment aspect when utilized on the CubeSat platform.

6.3 Bottom Feeding with Circular Ground Plane

Designing the bottom feeding conical log-spiral will be completed using the same methodology as the UHF version of the antenna. That is, a parametric study of the antenna will be performed with sweeps of the ground plane size/shape, height of the spiral arms above the ground plane, and impedance. Similar to the top fed conical log-spiral, this section will provide simulated results of the bottom feed setup of the conical log-spiral antenna.

6.3.1 Bottom Feed: Input Return Loss

The input return loss is optimized for values below the required -10dB. Antenna height and impedance are swept to satisfy the antenna requirements. Figure 6.6 shows the sweep of the antenna height above the ground plane, where the height that stabilizes the antenna is approximately 1cm or more. Sweeping the impedance with the height at 1cm can be seen in Figure 6.7. The increase in impedance reduces the maximum value for the return loss and guarantees that with some error the return loss will remain below the needed -10dB value.

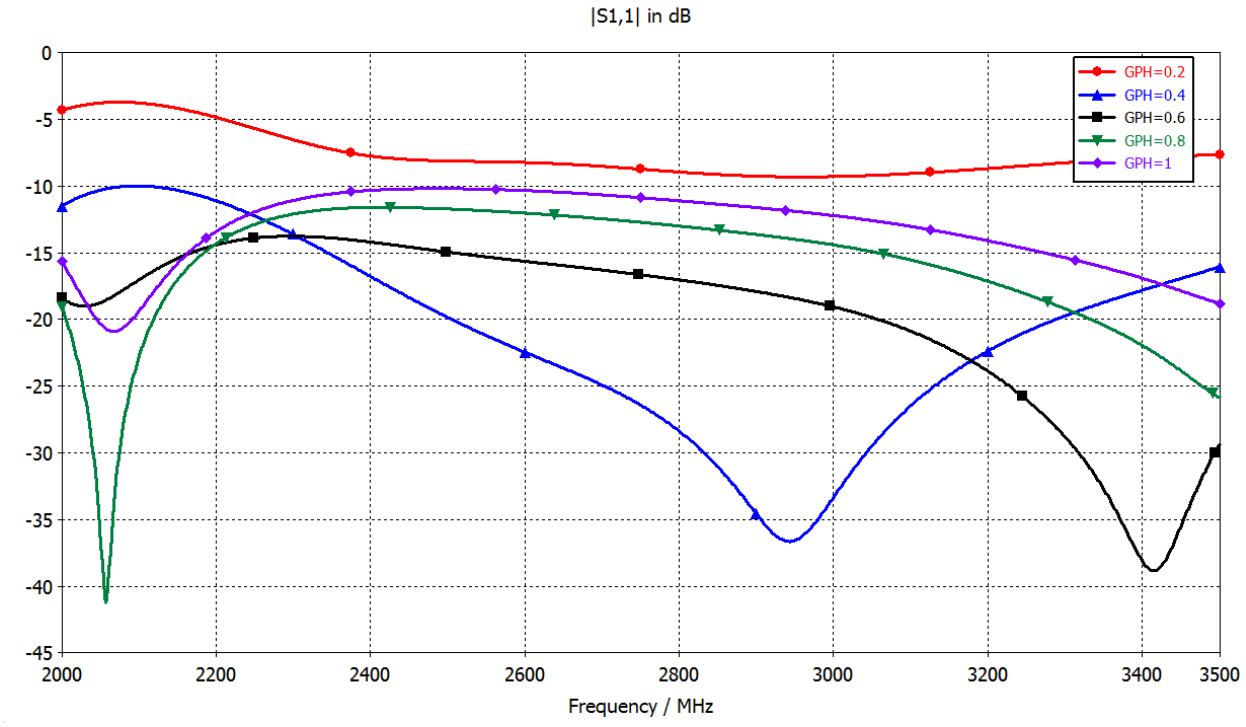

Figure 6.6 Return loss through a sweep of antenna height above the ground plane (seen as GPH in cm).

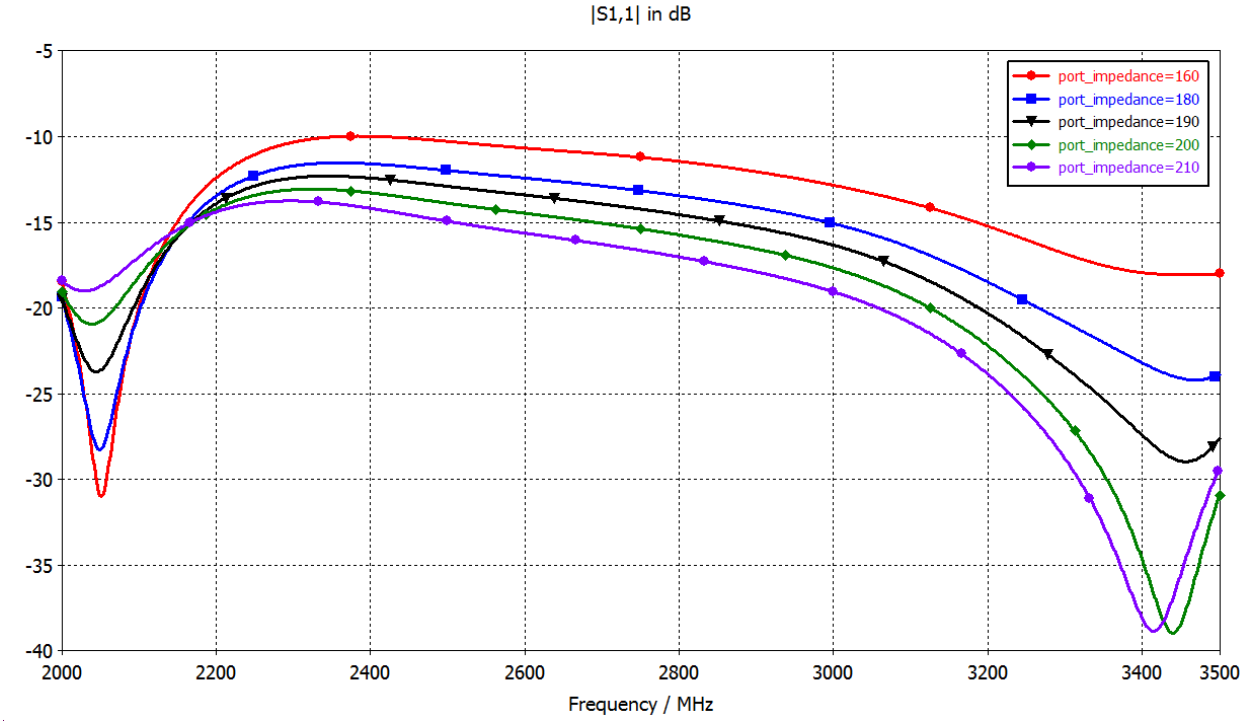

Figure 6.7 Return Loss through a sweep of the port impedance with ground plane radius of 8 cm and height of 1cm.

6.3.2 Bottom Feed: Far-Field Magnitude

Radiation efficiency of the bottom fed CLSA is close to unity or zero in decibels, with a slight deterioration at the band edges, as seen in Figure 6.8. The polar and 3D far-field results for the band edges are found in Figure 6.9 and Figure 6.10, respectively. These plots are consistent with the bottom fed UHF design of the CLSA presented in Chapter 5.

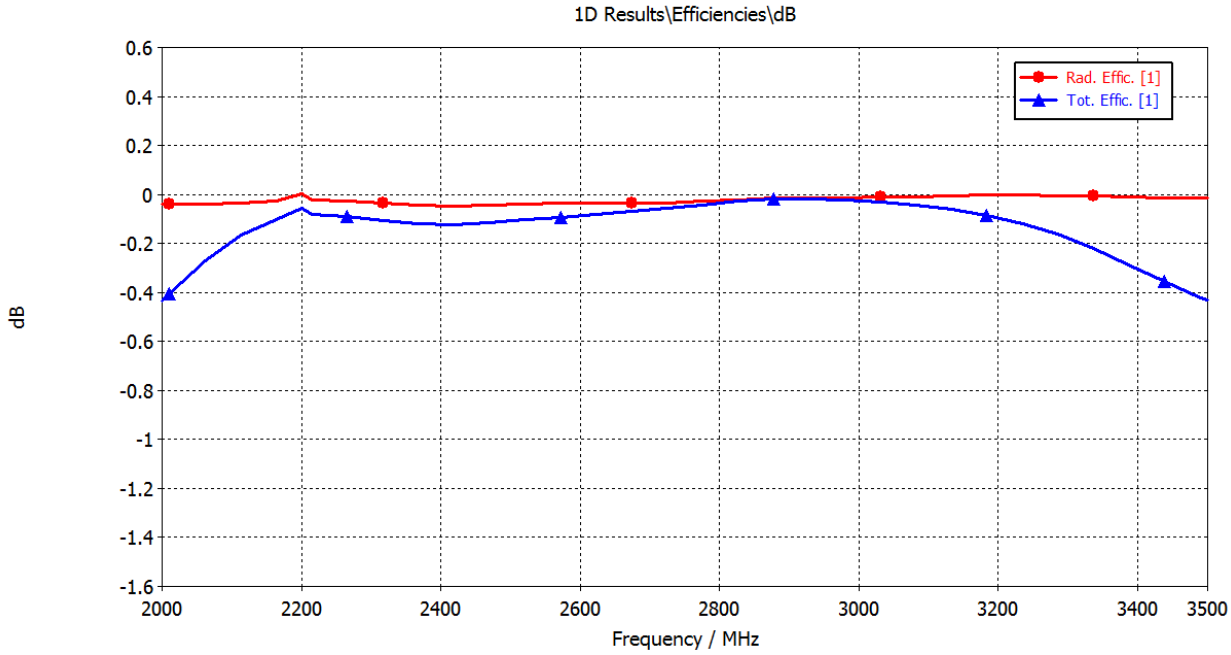

Figure 6.8 Radiation and total efficiency for the bottom fed CLSA.

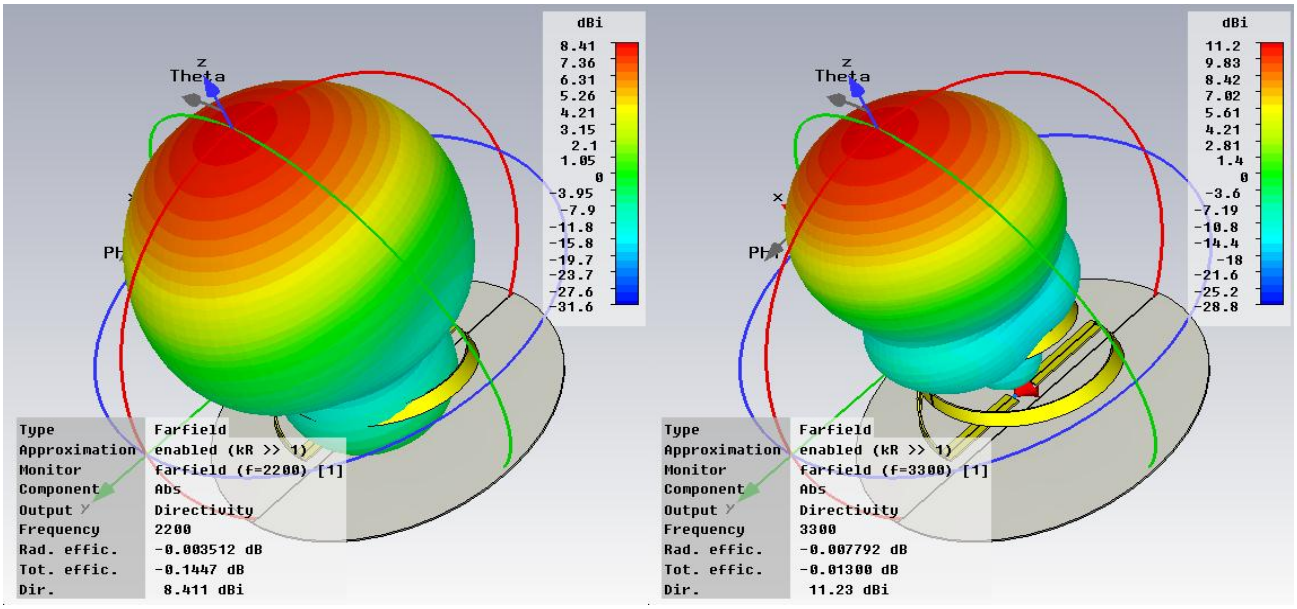

Figure 6.9 3D far-field directivity of the bottom feed CLSA at 2200MHz (left) and 3300MHz (right).

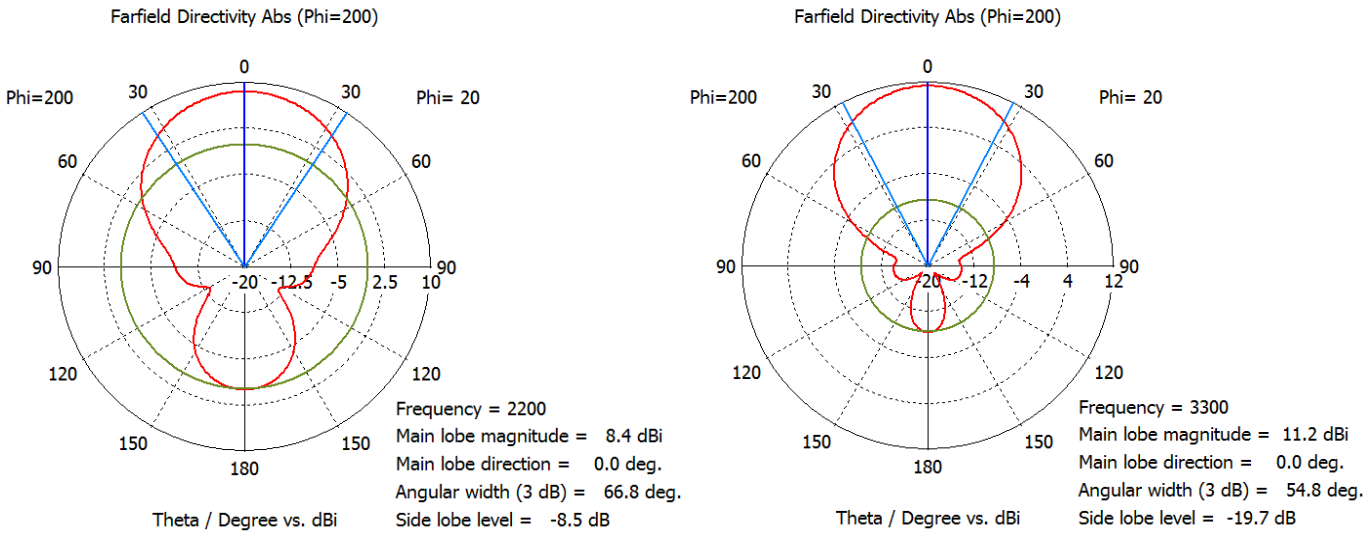

Figure 6.10 Polar cross-section of far-field directivity at 2200MHz (left) and 3300MHz (right).

6.3.3 Bottom Feed: Axial Ratio

The axial ratio found for the scaled version of bottom fed CLSA is similar to the design in Chapter 5. Axial ratios at the band edges are given in Figure 6.11. An axial ratio at the lower frequency of 5dB is postulated to be an artifact of the feeding system, as to be corrected within the construction of the antenna. Relating the 5dB axial ratio to the polarization loss with respect to an incident RHCP, located in Figure 1.1, the maximum polarization loss is only 0.5dB and can be included in the total gain.

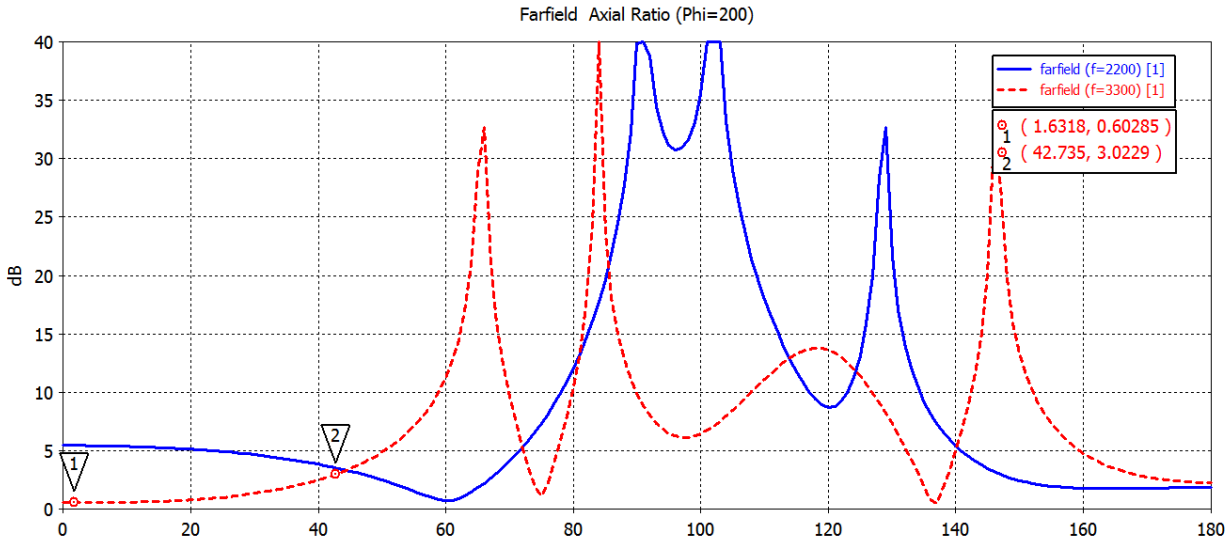

Figure 6.11 Cartesian plot of the bottom fed CLSA axial ratio at antenna band edges.

6.3.4 Bottom Feed Conclusion

Scaling the bottom feed UHF CLSA design did not have any major inconsistencies. The ground plane radius and antenna height above the ground plane scaled up in frequency with no distortions. Simulated results in the previous sections state that the S-band antenna is consistent

with and a prototype construction would reliably portray the characteristics of the UHF design. With this information the antenna is ready to be constructed; however the antenna feeding has not been evaluated and will be presented in Chapter 7.

CHAPTER 7

Feeding Mechanisms for Conical Log Spiral Antenna

Many times overlooked, the feeding system for any antenna needs to be carefully analyzed. The antenna within the simulation domain can have an assortment of feeding mechanisms to properly excite the radiating structure. The differential feed setup in the simulation is defined as "balanced" feeding. The term balanced is used to describe the phase difference of 180° seen at the two antenna arms. Therefore, the input into the antenna must have a balanced, or 180° phase difference, input to each spiral arm.

Design of the balun structure that matched the antenna requirements was attempted and due to fabrication limitations was not produced. Known fabrication limitations hold the designed

structure at a standstill, therefore another alternative is presented within this chapter. The alternative is a commercial balun with other designed attributes to offer the required performance demanded by the antenna. A design procedure for the commercial balun is presented with measured results. The results and possible limitations will be discussed.

7.1 Commercial Balun

Since most baluns researched are not balanced for the needed bandwidth or are limited by fabrication, the alternative is the use of a commercial balun [17]. One available for use was supplied; however the impedance is not matched to that of the antenna. The balun is a 50/50 balanced, which means that the input port is 50Ω while two output ports are 25Ω each. A 50/200 balanced component would be the best choice; however availability placed lead times in the three to four week range. A 50/200 balanced gives the proper antenna impedance of 200Ω. The balanced term implies that each arm will be 100Ω with respect to ground. The 805 chip balun can be placed on a microstrip circuit with modifications to the output to give the proper impedance.

An example of a divided, but in-phase, output ports would be the Wilkinson power divider with a 50Ω input. The two splitting arms are determined to be a quarter wave transformer (QWT) of impedance 70.7Ω, which is the value needed to transform a 50Ω line to a 100Ω line. However the two output ports are given an impedance of 50Ω. This is due to the impedance of each output line to ground, which is simply the transformed value of 100Ω. The same is true of the "differential" impedance of the antenna at 200Ω, with the phase difference exception of "balanced." The characteristics of the balun are given in the data sheet and

measured after the microwave circuit is constructed. The following sections provide the means for the impedance match, simulation characteristics, fabrication definitions, and measurements.

7.2 Impedance Transformation

Transforming the impedance is used by implementing a QWT. The QWT arises out of the simplification from the input impedance equation for transmission lines with a line of given impedance attached to a load [19]. The characteristic impedance is defined as the square root of the product of the impedances on either side of the transformer, when the line length is λ/4. Figure 7.1 shows the QWT on the balanced ports to transform the 25Ω impedance to 100Ω. The impedance of the QWT is thus 50Ω; a convenient value since standard impedance for many devices is 50Ω.

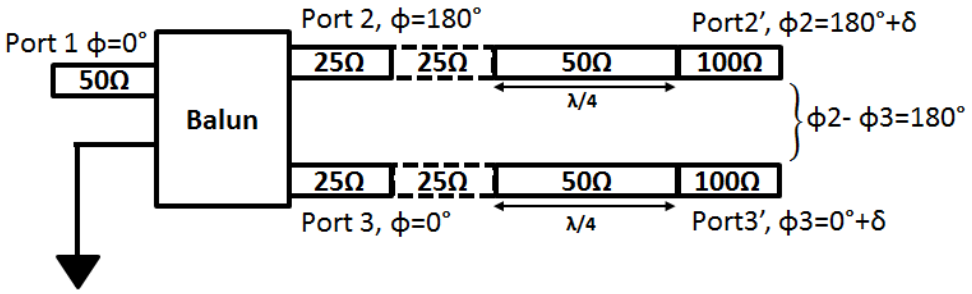

Figure 7.1 Balun and QWT circuit for 50/200 balanced transformer.

Other important aspects that need to be considered by the QWT are the phase balance of the two output lines and if they stay balanced with the impedance transformation. From Figure 7.1, the phase at the two output ports of the balun is 180°. The length of the transmission line is set at a quarter of the center frequency for the antenna at 2.75GHz. As the electrical length will

change with frequency, the two ports will still see the same electrical length; therefore the phase difference will stay the same regardless of the change in frequency.

To further prove that the transformer will provide the needed input RL, a simulation using an arbitrary microstrip substrate is performed in Agilent ADS. The setup of the test is using the theoretical transmission lines and implemented microstrip lines, as seen in Figure 7.2. Results of this analysis, seen in Figure 7.3, shows that the required bandwidth is achieved by the QWT in both of the models with respect to the input RL and IL. The match between the theoretical and the implemented microstrip lines are very close. The QWT is thus a simple, yet elegant, method to transform the impedance.

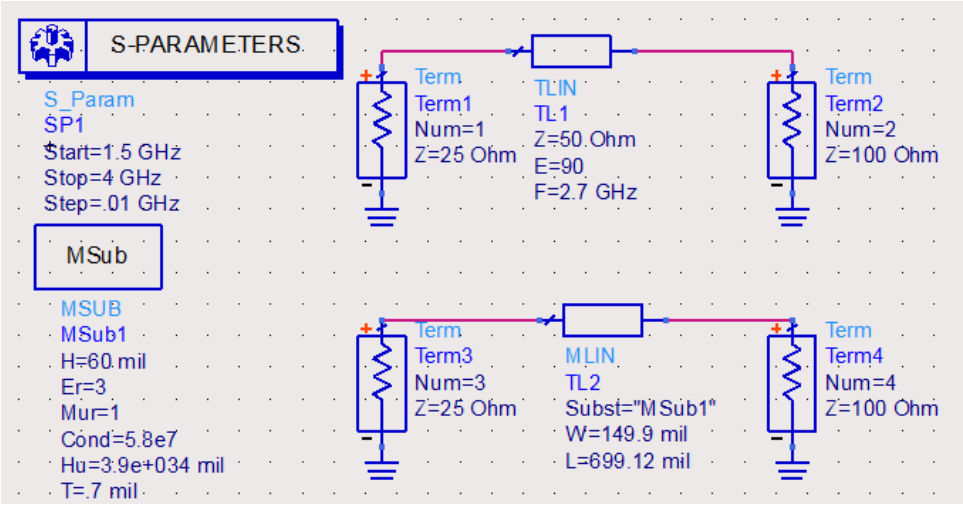

Figure 7.2 ADS simulation of a theoretical (top) and implemented (bottom) QWT.

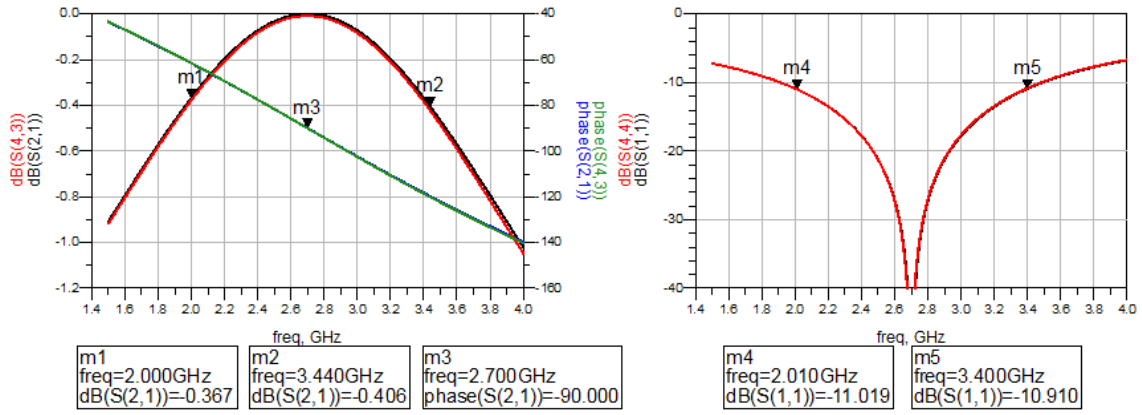

Figure 7.3 Results of the ADS simulation for the QWT.

7.3 ADS Simulation of Balun with Transformer

Combining the S-parameters and the QWT in a simulation will provide general guidelines to how the input RL will be measured when the antenna is connected. The bandwidth will be determined by the -10dB RL distinction. Using the S-parameter files for the balun from the manufactures website, a circuit with the QWT and 100Ω loads is created in ADS. Figure 7.4 shows the circuit used to test the balun parameters. It should be noted that the S-parameter file is based on typical values of the balun. The results of the simulation are given in Figure 7.5. The unfortunate fact about the balun is that the bandwidth is reduced to a band of 2.2GHz – 3.1GHz. Therefore the measured bandwidth of the antenna will be directly limited by the band width of the balun. Phase from the balun and the QWT is neatly at 180° $\pm$ 3°, which satisfies the balanced input requirement. Some additional insertion loss can be seen, with the typical value for the balun being 0.7dB. Also, the amplitude balance between the two output ports is within 1dB within the RL bandwidth. These results suggest that the performance of the antenna will be constrained by a direct relation to the performance of the balun. Given more time for the project, an adequate balun that consisted of the same 805 chip size would be acquired. Since the 3 - 4

week lead time is out of the time frame for the project, the limited results will be noted and the project will move forward.

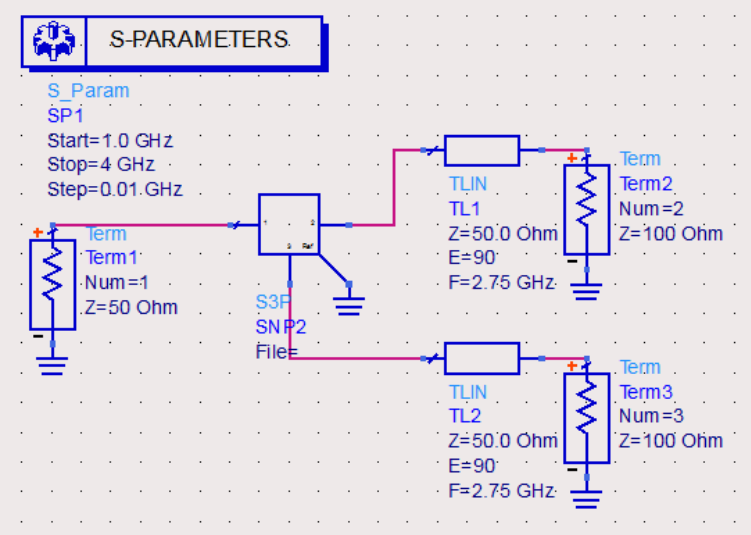

Figure 7.4 ADS circuit diagram for the balun and the QWT.

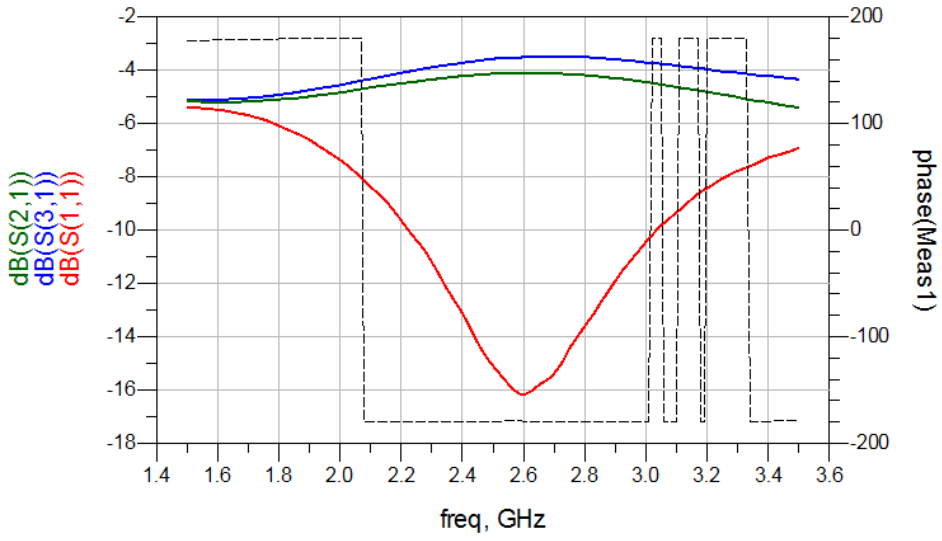

Figure 7.5 ADS simulated results for the balun and QWT. Jumps in phase are switches of positive and negative phase.

7.4 Layout and Fabrication

The determination of how the two output ports of the balun will be connected is discussed within this section. The use of 100Ω lines was determined by the procured 100Ω coaxial semi-rigid transmission lines. The 50Ω edge launch connectors add an unknown amount of electrical length, which would shift the center frequency of the QWT. With the use of 50Ω edge launch connectors out of the question for the balanced port, the alternative method is to launch off the balun board with the coaxial connectors. This is accomplished by adding grounding pads along the launch where the outer conduction of the coaxial line is soldered. Continuity of ground is preserved with this technique. The inner conductor of the coaxial line is then soldered to the microstrip line. As TEM field structures for both coaxial and microstrip are different, the method mentioned is crude, yet effective [19]. The two balanced 100Ω coaxial semi-rigid lines will feed the antenna from the bottom with the inner conductor being soldered to the antenna.

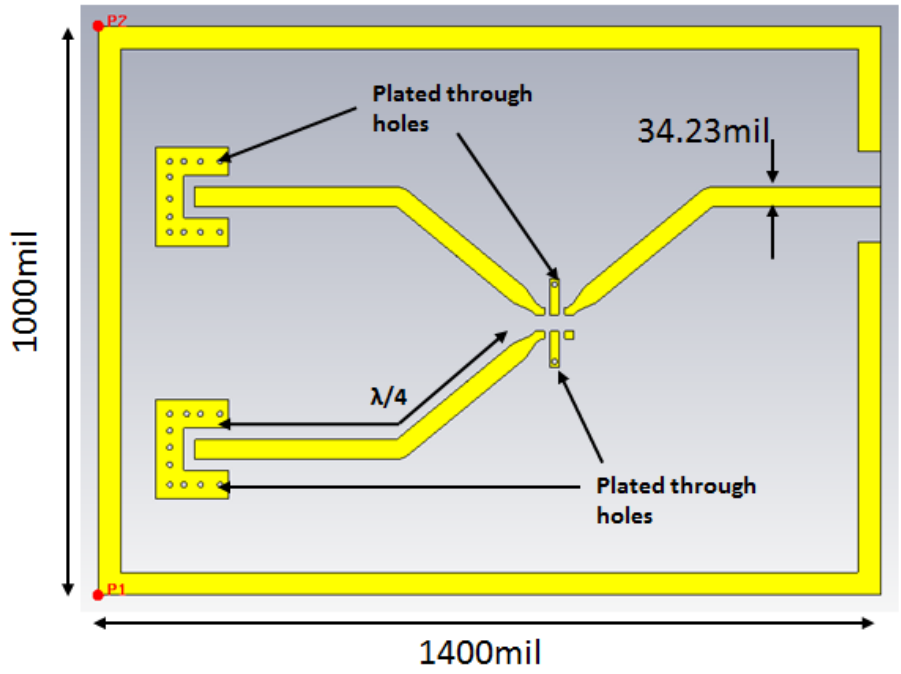

Figure 7.6 Layout of the balun board with the QWT and coaxial launches.

Layout of the microwave circuit for the balun is taken from the suggested layout located within the data sheet [26]. Width and length of the microstrip lines was calculated based on 0.4 mm (16 mil) of Rogers 4003 material. The relative permittivity of the substrate also plays a role in the microstrip width and length. Tapering the 50Ω lines to the balun pads are seen in Figure 7.6, which are inserted due to the fact that the pad and the width of the trace are not the same. Fabrication starts with the substrate between two layers of copper. The top layer is chemically etched away and leaves the pattern seen in Figure 7.7. This topic is discussed further in Chapter 8.2. Plated through holes give a connection to the ground layer, the side in which the copper was not chemically etched. The metal plated through holes, called "vias", are needed for the balun chip, as portions need to be connected to ground for proper function. The vias are also used to connect the outer conductor of the semi-rigid coaxial line to ground, as seen in Figure 7.8. The figure also shows the chip balun and the 50Ω soldered launch connector soldered to the board. Additional copper backing was placed under the semi-rigid components for extra support.

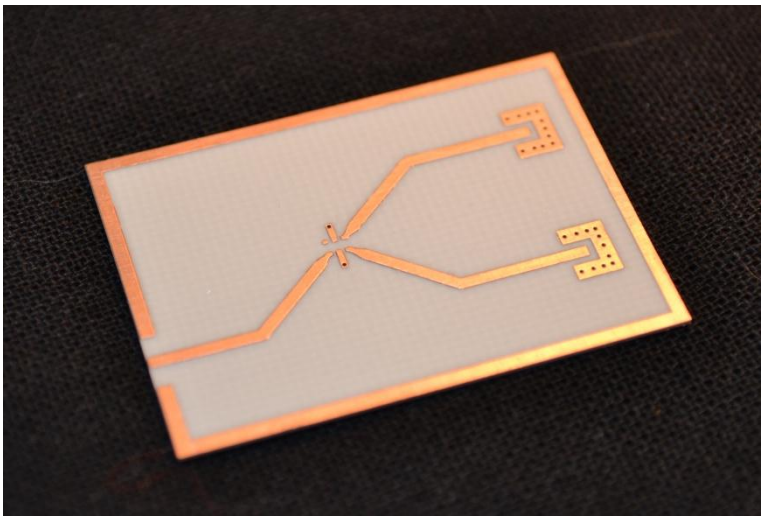

Figure 7.7 Fabricated balun board for use as the antenna feed.

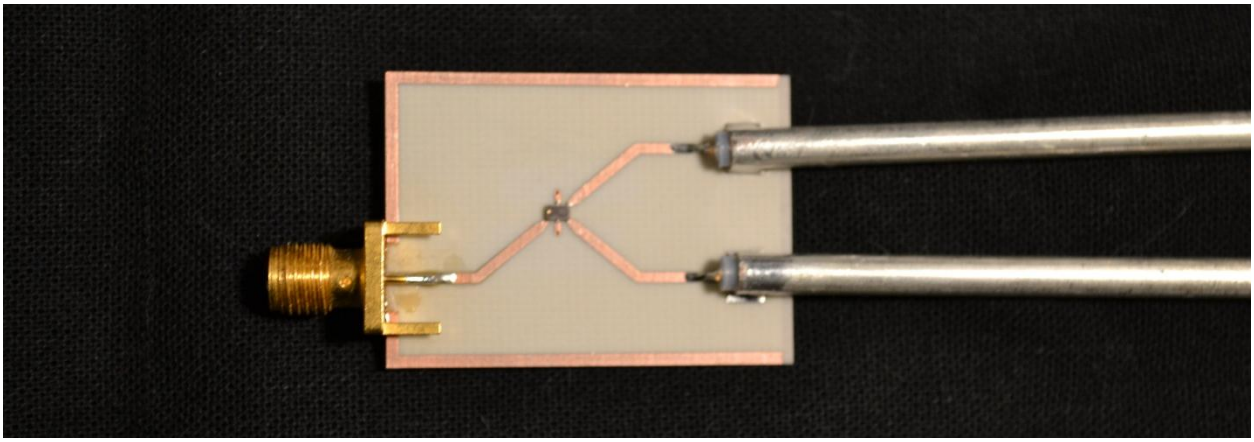

Figure 7.8 Constructed feed that includes the 50Ω launch connector, balun, and two 100Ω semi-rigid improvised coaxial launches.

7.5 Measurements

The best way to measure the constructed balun circuit would be to have a 50Ω system on port 1 input and a 100Ω system on port 2. Unfortunately this best setup is not available given typical network analyzers, which measure the incident and transmitted power on a port to port basis with a defined impedance. Given the nature of the three port balun, two 100Ω resistors were soldered at the output of the QWT to grounding pads, as seen in Figure 7.9. This enables the RL to be measured within a 50Ω system and not converting impedance mismatches and loading issues when trying to measure the full three port S-parameters of the balun board. The measured return loss of the 100Ω loaded board and the simulated balun and QWT are given in Figure 7.10. These results give a larger bandwidth and better minimal RL. As evident of the measurement, the feed system is highly dependent on how the loads on the outputs are balanced. Keeping this aspect of the three port balun circuit in mind, the antenna must be constructed and only then can the true measurement of RL be completed.

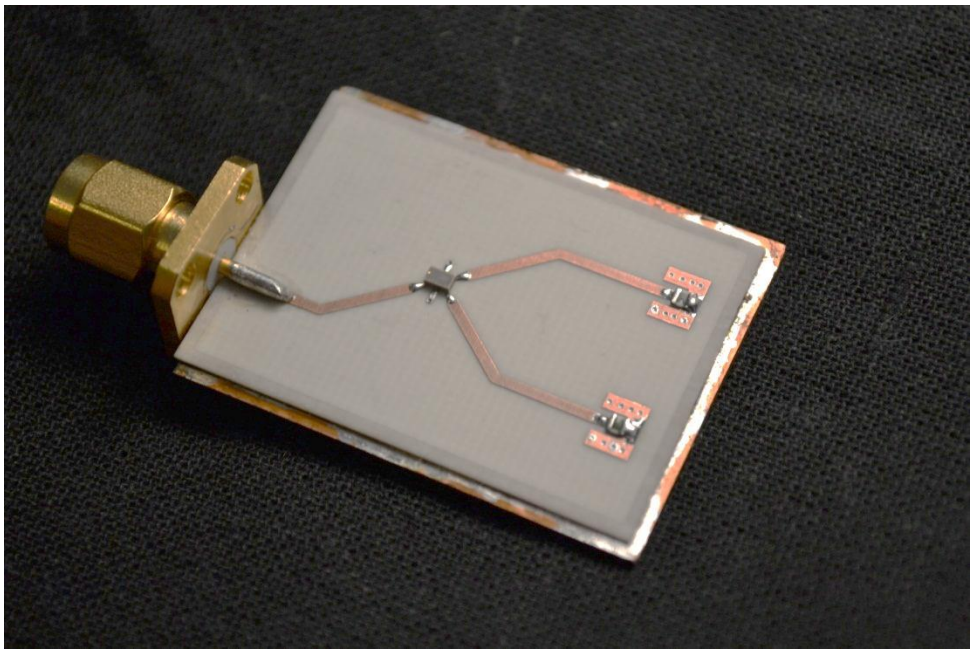

Figure 7.9 100Ω loaded balun board for accurate RL measurements.

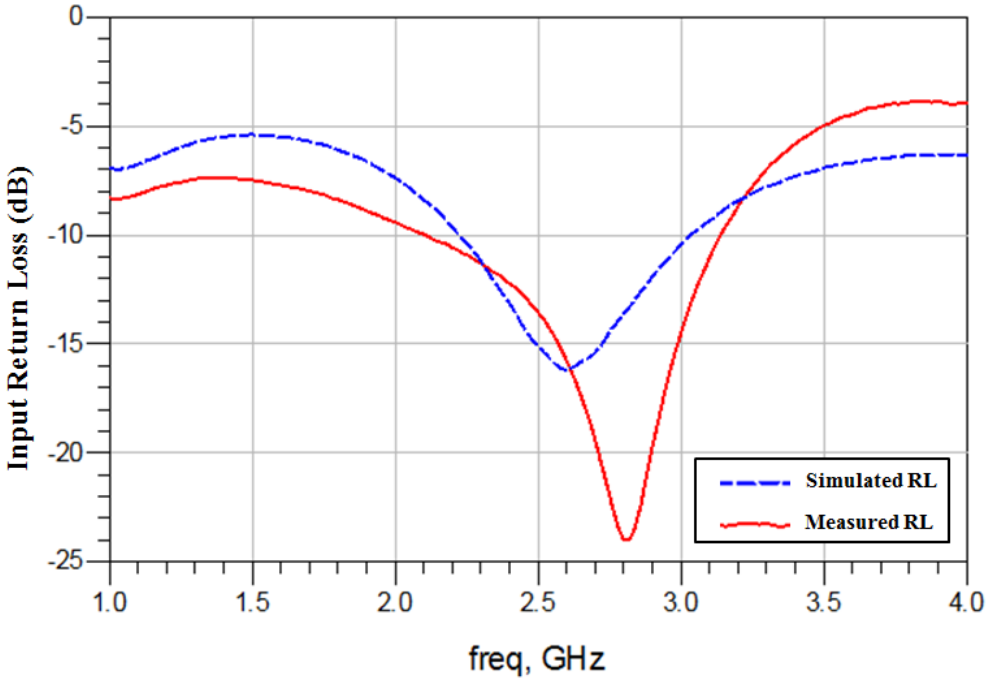

Figure 7.10 Simulated verses measured input RL of the balun board.

CHAPTER 8

Construction of the CLSA and Feed Integration

To test the simulated results, the construction of the log-spiral antenna is to be completed. Major challenges for building the antenna are the accurate rendering of the spiral arms and making them match the equations presented in Chapter 3. Since the dimensions define the active region, and thus the radiated fields, extreme caution is necessary to model the antenna correctly. From the work of Dyson, it is not clear exactly how the CLSA's were build. There are mentions to using "copper clad Teflon impregnated fiberglass" that was etched to form the spiral arms [14]. Without the facilities to accomplish this method of fabrication, alternative methods will be explored.

8.1 Unwrapping the CLSA

Given that the spiral arms are planar copper strips wrapped around a defined conical structure, the sheets can be given in a planar form, similar to other sources [23]. Some examples of this would be transforming the governing equations in Chapter 3 into a two dimensional form that can be fabricated. Options for fabrication will be presented in the following sections. First the transformation from the three dimensional CLSA to planar version must be investigated.

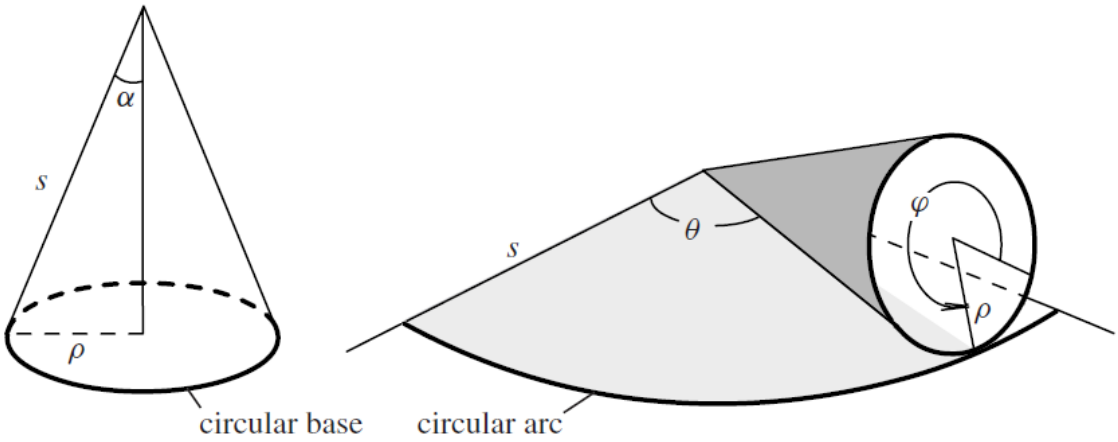

Figure 8.1 Unwrapping the conical surface on a 2D plane [24].

The ability to have the exterior of the conical structure on a planar surface would make fabrication an easier process. Once the spiral arms are printed on a copper surface, the trace can be cut or etched out. The preservation of the arc needs to be preserved to have the same spiral arms when they are wrapped back around the conical surface. Figure 8.1 shows an example of how the face will be unwrapped onto a planar surface. To accomplish this from the simulation antenna, the total length will be needed. By selecting the edge of a spiral arm in CST, the length is given as 28 cm (11 in). The total length travelled along the antenna arm will need to be the

length of the planar curve, which will be extended to ensure that enough of the spiral is intact to be rewrapped on the cone. Only a slight modification is need to the analytical face in CST, where the z-component of the equations will be dropped and replaced with a constant. The constant will describe where the planar face intersects the z-axis.

As the cone is unwrapped, only a portion of the full circle is swept. To get the spiral as a single strip of copper, the remaining revolutions must be applied by further unwrapping the face from the cone. Multiple revolutions around the cone will be swept as the rotating cone forms a circle. Applying the modified equations in CST gives the results of a planar equiangular spiral, which is the unwrapped version of multiple revolutions around the cone as seen in Figure 8.2.

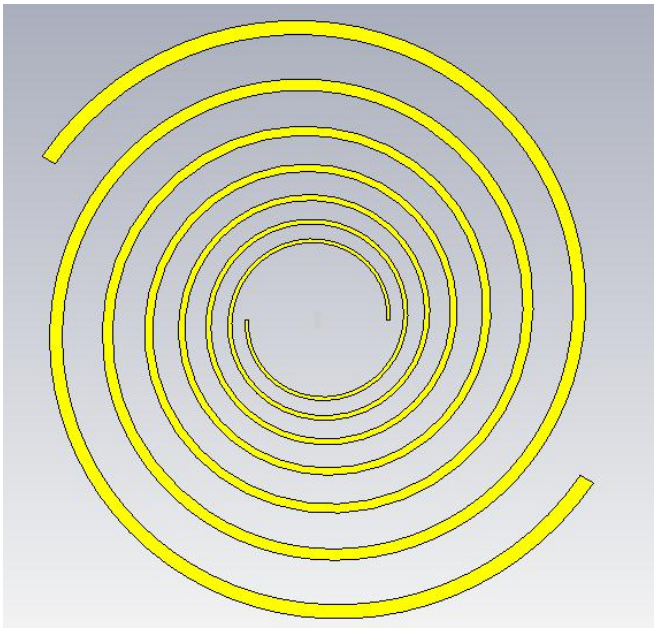

Figure 8.2 Unwrapped spiral arms in a single plane.

8.2 Planar Fabrication

Exporting a single layer file from CST is necessary to fabricate the design created. The process by which the spiral pattern is removed from a copper sheet is called chemical etching for printed

circuit boards (PCB) [25]. A negative image of the planar spiral shown in Figure 8.2 is printed on a layer of "photo resist". This layer is immune to the chemical that dissolves the exposed copper layer. This photo resist is then applied to a sheet of copper and then submerged in a bath of ferric chloride or another copper solvent. As the resist is not affected by the solvent, the portion of copper under the resist forms the remaining copper image. Figure 8.3 shows the completed process, which took place at a local PCB shop. The extra copper attached to the spiral arms is used to "tie in" the design so it does not fall through during the etching process.

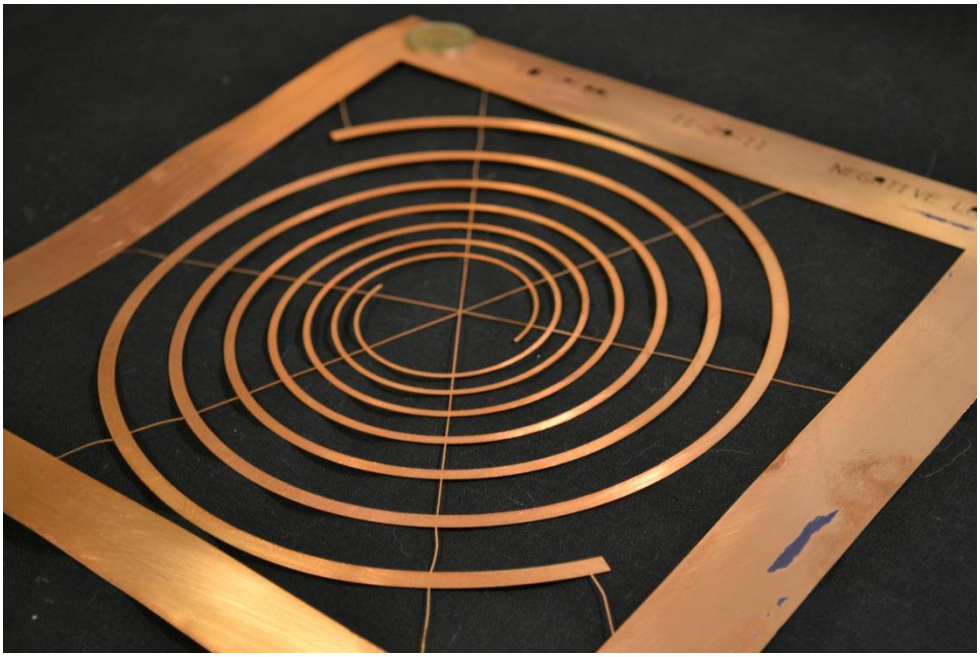

Figure 8.3 Printed form of the spiral arms through a chemical etching process. Excess copper is present to "tie in" the spiral arms so that they do not fall during the chemical etch.

8.3 Antenna Construction

The antenna is contructed with the aid of a printed 3D cone that fits the dimensions given in Chapter 6. The plastic cone was created in a 3D printer that takes data exported from CST. The printer, using granular binding, starts from the base and selectivly fuses print media to form the

desired conical shape. From the CST design, points along the cone are marked to show where the spiral arms are to be placed on the surface of the cone. The introduction of the cone initialized several additional simualtions to see the effects. Those are seen at the end of this Chapter. Cutting the excess wire from the fabricated spiral arms, the antenna is wrapped around the cone to form a similar structure compared to the simulation. Forming the spiral arms exactly is a patient task, where some additional adhesive was needed to keep the copper arms stable. Figure 8.4 shows the comparison of the CLSA in the simulation domain, left, and the constructed antenna, right. During construction it was noticed that the width of the arms was not exactly those given in the simulation. It can be concluded that the differecne in width is an artifact of the transformation process to a planar printed structure. Future work can improve the transformation process, as this small anomoly is due to the growth rate of the spiral arm width and should cause minimal field deteriorations [13].

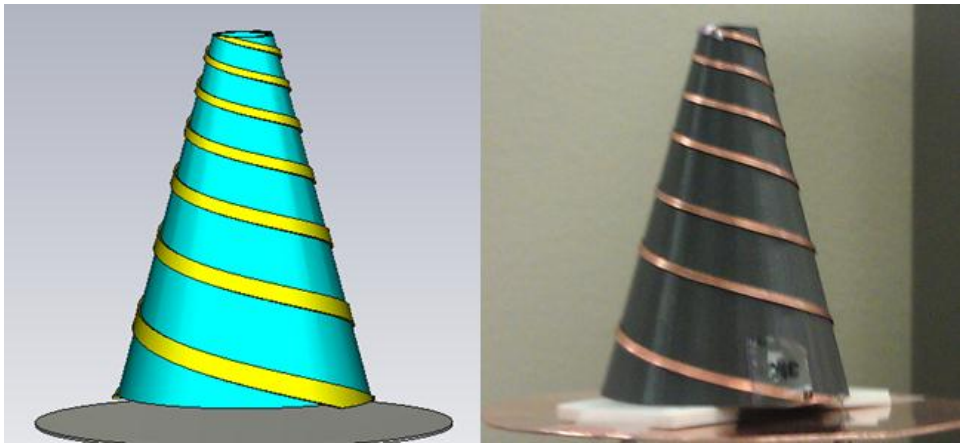

Figure 8.4 Comparison of the simulation (left) and constructed (right) CLSA.

A gound plane is needed next and was created using a solid sheet of thick copper that was cut into a circular form. The antenna will sit on top of the ground plane at a distace of 2cm

above. Since the balun circuit is on a separate portion of the design, the connection between the two must be resolved. Discussed in Chapter 7, the balun has 100Ω semi-rigid coaxial lines that take the balanced feed lines off the balun board. Two holes, the size of the 100Ω coaxial cables are drilled through the copper ground plane. The coaxial lines will then be inserted through the drilled holes to provide antenna feeding. The lines are then soldered on the feed side of the ground plane, as seen in Figure 8.5. Ensuring that the inner conductor of the coaxial line is exposed, the two lower spiral arms are soldered to these inner conductors, thus completing the combination of the antenna and feed system. By soldering the coaxial inner conductor to the antenna arms the current should flow up the arms, as intended and seen within the simulations. The foam seen in Figure 8.4 is to support the antenna and should not cause any disruption in performance, since the relative permitvity is close to unity.

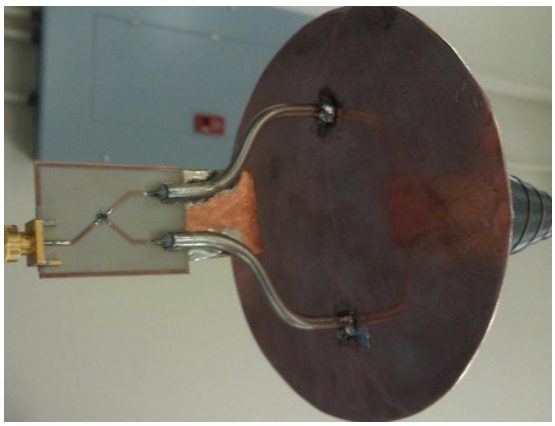

Figure 8.5 Feed assembly attached to the antenna ground plane.

8.4 Additional Cone Effects

The introduction of the plastic cone is for support of the spiral arms. This plastic cone could have some side effects on the input return loss and radiated fields, as the relative permittivity is

not unity. Through the published characteristics of the plastic used in the 3D printing process, the relative permittivity is not listed. Therefore the plastic cone is given several permittivity values to ensure return loss and radiation pattern performance is not disrupted. Going through several parameter sweeps, the results in Figure 8.6 and Figure 8.7 show only slight frequency shifts and pattern enlargement consistent over the bandwidth. Thus, the antenna system is ready to be tested.

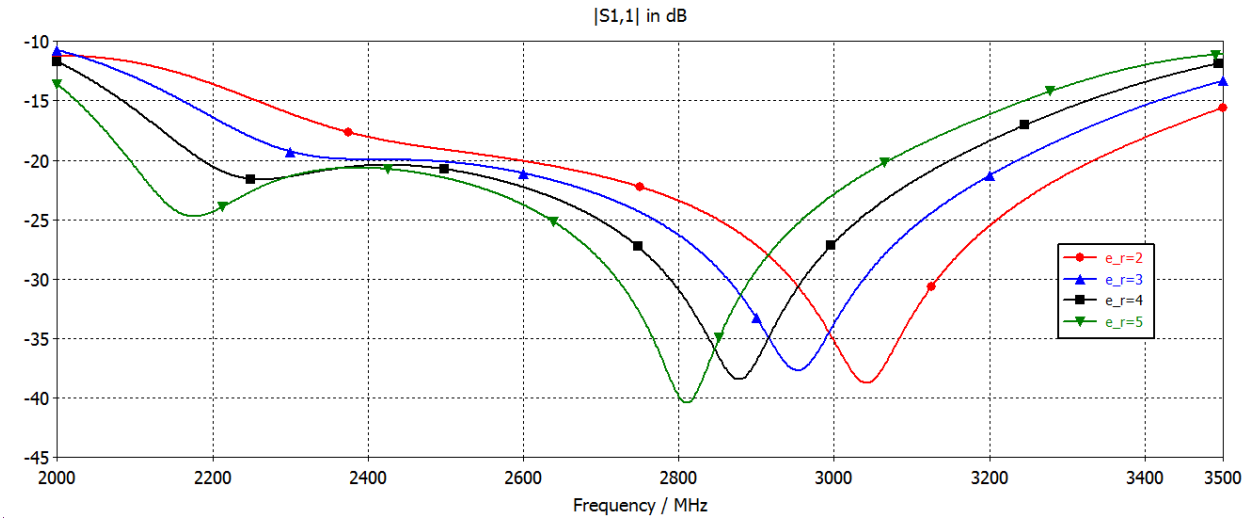

Figure 8.6 Input RL through swept relative permittivity of the cone shell.

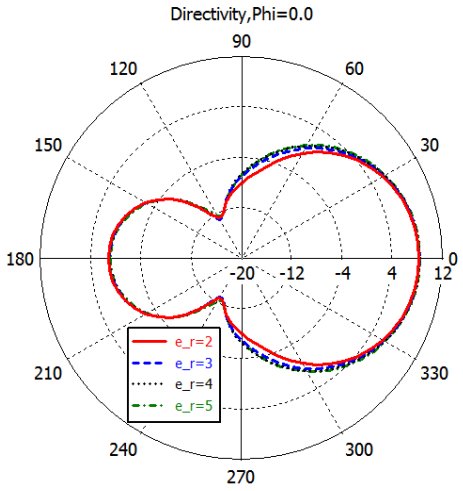

Figure 8.7 Typical polar cross-section of far-field directivity through swept relative permittivity of the cone shell

CHAPTER 9

Results

The results of the fully constructed antenna are presented in this chapter. This includes the setup procedure for included tests, the measured results, and an analysis for each measurement with respect to the simulated version. Three measurements setups will be given, which include the input RL, radiation pattern, and gain measurements. The input RL is measured with a network analyzer, where the input of the feeding system is connected for a single port measurement on the network analyzer. Radiation patterns are taken by revolving the CLSA while another antenna is transmitting a continuous wave (CW). A computer program then records the power level as a function of the rotated azimuth angle. The last measurement is the gain of the antenna, which is calculated by the Friis transmission equation. The Friis transmission equation is used with the known gain of the standard antenna, the transmitted power of the gain standard antenna, the free space path loss, and the measured power from the CLSA. The only unknown is the

receiving antenna gain and is easily solved. All of these testing procedures will be described in detail within their respective section.

9.1 Input Return Loss

As with finding the input return loss of the feed system in Chapter 7, the total antenna structure now has one input port. The input port is connected to the network analyzer, which gives the results seen in Figure 9.1. The measured feed RL is included with the figure for comparison. The total band width of the antenna is measured to be 2.2GHz -3.1GHz, which is a direct relation to the bandwidth of the balun in the feed system.

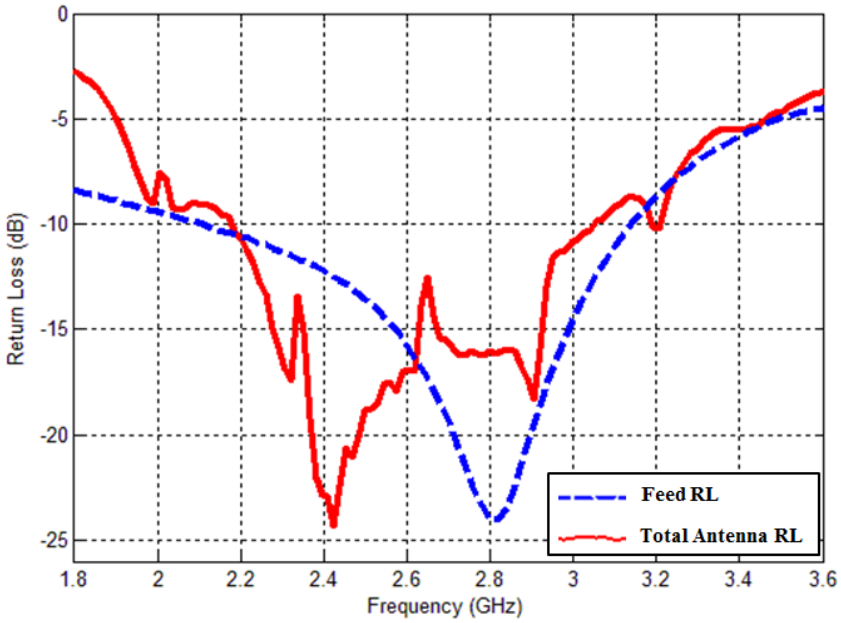

Figure 9.1 Measured input RL of the total antenna system verses the balun feed.

Major difference in the two measurements is the shift of the minimum RL value down in frequency. Many factors can lead to this shift; however it would be difficult to decouple the antenna and the feed system to both simulated values. With the given results the antenna is

matched within the bandwidth of the balun, but whether it radiates the simulated pattern is to be seen in the following sections.

9.2 Radiation Pattern

Proper radiation pattern measurements are completed in what is called an anechoic chamber. The anechoic chamber is lined with pyramids of radiation absorbent material (RAM). RAM within the anechoic chamber reduces the reflection of an incident wave and in turn makes the testing antenna only "see" what is transmitting from the gain standard. The CLSA is mounted on a rotating fixture that revolves about the azimuth angle and connected to a computer program that records the measured signal, as seen in Figure 9.2 and Figure 9.3.

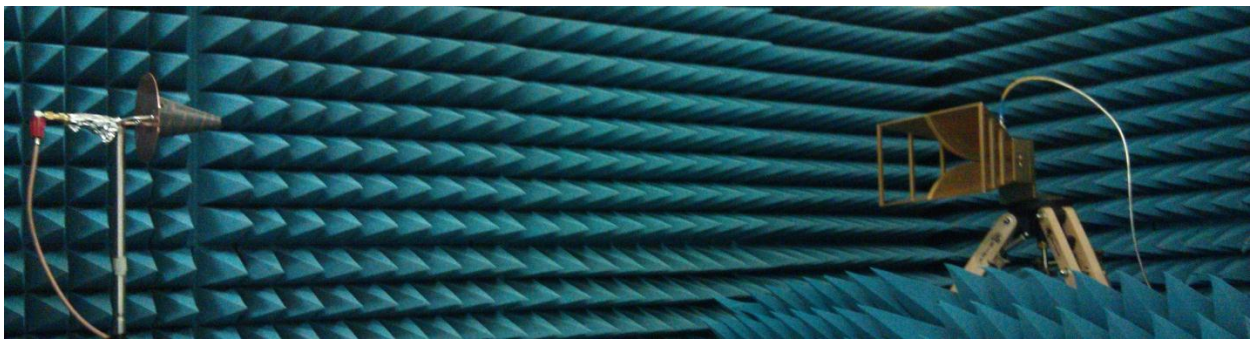

Figure 9.2 Configuration of the gain standard antenna and the bottom fed CLSA within the anechoic chamber.

Received power is not measured by the computer program; however it has a dynamic range of -40dB to 0dB. When reading 0dB in the program, the received power is not 0dBm. Therefore for each frequency the transmitted power from the gain standard antenna is changed so that the maximum signal seen on the computer program is 0dB. This guarantees that the full dynamic range is used without clipping the signal on either threshold. Received power cannot be

measured through the program and will be considered in the next section. The gain standard antenna is connected to a signal generator that outputs CW, also known as a tone, through a coaxial connection. Power level and frequency of the tone can be modified on the front panel of the signal generator. Even with a lack of "known" received power, the program is calibrated at each frequency step by changing the output power of the signal generator until the program reads 0dB. Measured and the simulated radiation patterns at each frequency step are normalized to zero and plotted in Figure 9.4.

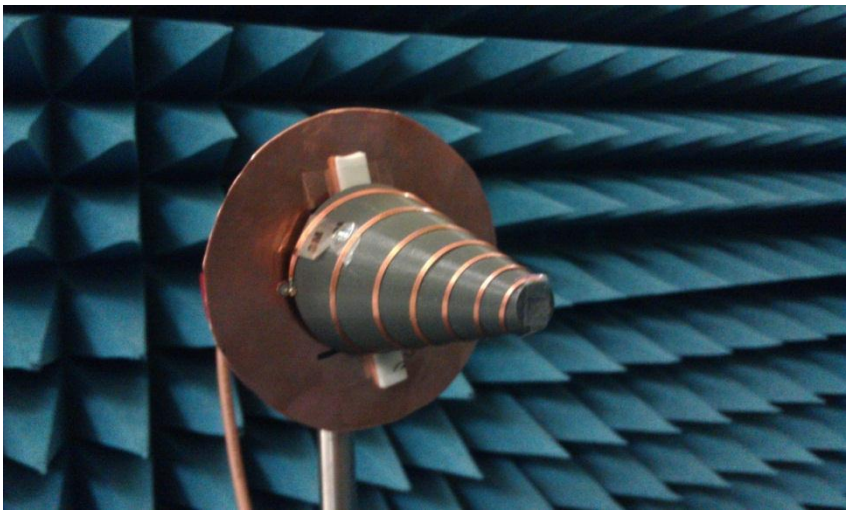

Figure 9.3 Mounted bottom fed CLSA in the anechoic chamber.

The patterns are normalized to form a pattern comparison between the measured and simulated antennas. Comparing the simulated and measured patterns, it can be seen that the main beam is consistent, while there is a reduction of the measured back lobes. This is due to the feed system that was not present in the simulated version of the antenna. It is also noticed that the main beam is closer to the simulated version at the higher frequencies of operation.

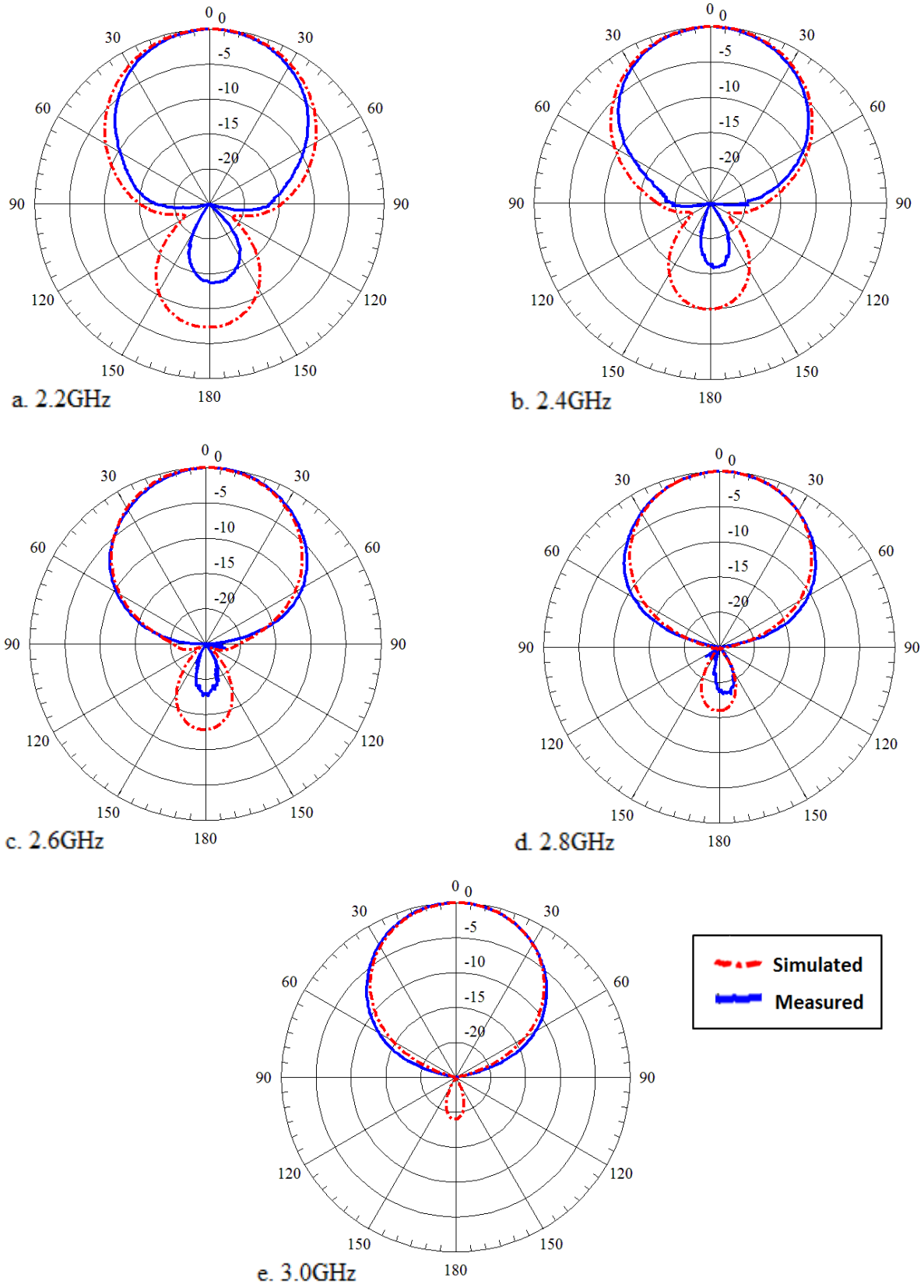

Figure 9.4 Normalized measured and simulated patterns (a) 2.2GHz, (b) 2.4GHz, (c) 2.6GHz, (d) 2.8GHz, and (e) 3GHz

9.3 Gain

The peak gain of the two cross polarizations will be measured in this section. The test setup is still within the anechoic chamber, where the gain standard antenna is rotated to provide vertical and horizontal polarizations for the approximate measure of circular polarization. Without a RHCP gain standard, the missing component in these tests will lack the imaginary phase term associated with the electric fields for circular polarizations. This is due to the linear polarization of the gain standard, where the phase cannot be physically introduced into the test setup. Assuming the cross polarizations give a good static approximation, the polarization loss can be deemed as 3dB.

The signal generator provides the CW with power and frequency control. To measure the received power a spectrum analyzer is connected to the feeding port of the antenna system. The spectrum analyzer measures the power across a frequency spectrum. The CW produced by the signal generator will not be affected by the resolution bandwidth, as the signal is a single frequency. Gain for this section is also affected by the antenna feeding, where the bandwidth is limited. Using the limited bandwidth should be sufficient in keeping errors in the gain calculation to a minimum. Utilizing the Friis transmission equation and solving for receiver gain, the following equation is formed [11]:

$$G_r = P_r - P_t - G_t - 20\log\left(\frac{c}{4\pi f D}\right)$$

Where G_r is the receiver gain, P_r is the receiver power, P_t is the transmitter power, G_t is the transmitter gain, and the last term is free space path loss (FSPL) at a measured distance of 1.21 m (4 ft). Along with all of these variables, the cable calibrations for loss must also be made.

Calibrating for these values was completed with the network analyzer in the frequency band of interest. Values that need to be added to the right hand side of the Friis equation are the losses from the antenna to the input of the spectrum analyzer, which includes polarization loss, cable loss, and feed insertion loss. Values that need to be subtracted are the losses from the gain standard antenna to the signal generator, which only includes the cable loss. Implementing the Friis transmission equation with the associated calibrations, Table 9-1 is created. The simulated peak gain is also given in the table for comparison.

Table 9-1 Measured bottom fed CLSA gain from Friis equation compared with simulated gain.

Pol (V/H)	f (GHz)	P_r(dBm)	G_t (dBi)	P_r (dBm)	FSPL(dB)	G_r (dBi)	ΔVH (dB)	Simulated G_r(dBi)
V	2.2	9	8.9	-15.6	-41.02	7.52	-	8.19
H	2.2	9	8.9	-16	-41.02	7.12	0.4	8.19
V	2.4	9	8.8	-14.9	-41.78	9.07	-	8.85
H	2.4	9	8.8	-15.3	-41.78	8.67	0.4	8.85
V	2.6	9	9	-15.4	-42.47	9.07	-	9.45
H	2.6	9	9	-15	-42.47	9.47	0.4	9.45
V	2.8	9	9.6	-14.5	-43.11	10.01	-	10
H	2.8	9	9.6	-14.5	-43.11	10.01	0	10
V	3	9	9.2	-15	-43.71	10.51	-	10.53
H	3	9	9.2	-15.3	-43.71	10.21	0.3	10.53

Gain values of the measured CLSA are seen to be approximately the same value as the simulation. Many factors could have caused the minor differences including errors in the spectrum analyzer, signal generator, loss calibration, and the gain standard antenna not being

consistent with published values. However the results are close to what was expected from the simulation, which proves that the antenna can be adequately modeled within the simulation.

9.4 Conclusions

The results presented in the section provide the necessary proof that the bottom feeding scheme was a success and can be implemented as an alternative feeding mechanism for the CLSA. Some effects of the ground plane are seen in terms of the beam width and gain, but these are due to the reduction of the back lobe associated with the top-fed version of the CLSA. Comparing the simulation of the bottom feed scheme and the results within this chapter, the correlation can be clearly seen. Thus, the prototype bottom fed CLSA paves the way for the UHF version to be applied to the CubeSat platform.

CHAPTER 10

Conclusions

The CubeSat platform is a well-defined structure with universal applications that reduces integration time and resources. The emphasis for this thesis was the design, simulation, and fabrication of an antenna that satisfies the characteristics and deployment requirements laid out in Chapter 1. A conical log-spiral antenna was chosen based on these given requirements and the antenna's ability to satisfy them. The CLSA also has the ability to be compressed and deployed on the CubeSat platform with minimal support structures given the proper alignment of the constructed antenna.

A major fault of the typical CLSA antenna design is the feeding location, which is at the apex of the antenna cone structure. This makes deploying the antenna difficult, since the

challenge is to support the feed and the antenna. Therefore a novel feeding location was devised to remove feeding support structures to the conical apex. This new feeding concept, which is located at the bottom of the antenna, requires a circular ground plane that is approximately the height of the antenna to redirect the backfire radiation away from the CubeSat assembly. The designed bottom fed CLSA was frequency scaled and prototyped to obtain an analysis of the new feeding performance.

The prototype of the bottom fed CLSA preformed analogous to that of the simulated results, proof that the antenna feed does not have to be located at the apex of the antenna. The measured results were limited by the chosen balun, a situation that can be easily remedied with a proper commercial or designed component. Results that were not hindered by the balun system meet expectations. With the prototype successful, further aspects of the design can be explored through future work.

Future Work

This thesis has presented a unique approach to a distinct antenna design with applications relevant to the CubeSat platform. Although the results for this thesis are consistent with the scaled prototype, much work would need to be completed prior to installation on a CubeSat. The work consists of enhancing the design and possible examination of redesigning the antenna to better suit the bottom feeding scheme. The following section presents the possible improvements and tasks to be considered for follow on work of the presented bottom fed CLSA.

10.1 UHF CLSA Construction Methodology

Constructing the UHF version of the antenna is an issue that must be resolved, as the CLSA proved to be a challenge to construct out of a planar approach. If the planar method is better suited for deployment, the width of the wire issue must be determined. Slight modifications to the planar version in CST can be made with minimal interference to the overall design. Since the UHF design is much larger that the prototype presented in this thesis, special considerations must be made to guarantee that the structure of the spiral arms remains intact.

Additional research into this area is needed if the metal of the antenna is to be formed on the defined conical surface, as the ease of an already processed antenna would reduce the errors of creating the antenna by hand. This type of construction needs to be space certified and the conical structure removed such that the antenna can be compressed prior to launch and then later successfully deployed.

10.2 Modification and Improved Modeling

The possibility for further investigating the bottom feeding antenna and improving the design is an option that can be determined before any construction begins. With the aid of simulation software, changes to the presented design can be accomplished in a reasonable amount of time to further study modifications to the original CLSA, beyond that completed within this thesis. Options to better model the design include the introduction of two separate coaxial ports feeding the CLSA through the ground plane instead of a single discrete differential port. With a fully

parameterized model constructed in CST, there are many avenues that can be discovered and analyzed.

10.3 Support Structures

The prototype employed a plastic cone for support; however the UHF design will not be able to construct a larger plastic cone. Support for the antenna structure will have to be a joint effort between deployment and microwave engineers to guarantee that the antenna gives the same characteristics as the simulated version.

Some initial exploration of the subject suggests that one option is the use of memory metals, made up of NiTi, to retain the needed shape of the spiral arms. The antenna shape can be "programmed" into the wire by a quick heating and cooling process. Challenges to this method would be the conical mold needed to withstand the heating and cooling process. One idea is the formation of a ceramic mold to hold the wire in place during the heating and cooling. Radiation efficiency has not been considered for NiTi in antenna design and may be a limiting factor for use with the CLSA.

10.4 Balun Improvements and Antenna Integration

The balun used had an inadequate bandwidth compared to the designed antenna. Improvements for this would include a balun that is designed or commercially procured. With the layout

completed within CST it would be a relatively small task to replace the balun with a similar size component.

Another aspect of the balun board that could be better is the implementation of the coaxial feeding as vias that go through the board's ground plane to the bottom of the spiral arms. The ground plane for the antenna could be doubled with that of the fabricated balun board. Typically this type of integration reduces the size of the overall system, as the route of the signal path is minimized. Prototyping of this type of feeding would have to be investigated prior to implementation.

REFERENCES

[1] A. Toorian, E. Blundell, J. Suari, R. Twiggs, "CubeSats as Responsive Sattelites", *3rd Responsive Space Conference*, 2005.

[2] C. A. Balanis, "Antenna Theory Analysis and Design 3rd Ed", *John Wiley & Sons*, Hoboken, NJ, 2005.

[3] J. D. Taylor, "Introduction to UWB radar systems", CRC Press 1995.

[4] A. C. Ludwig, "A simple graph for determining polarization loss", *Microwave Journal*, vol 19, no 9, September 1976.

[5] S. Gao, K. Clark, M. Unwin, J. Zackrisson, W. A. Shiroma, J. M. Akagi, K. Maynard, P. Garner, L. Boccia, G. Amendola, G. Massa, C. Underwood, M. Brenchley, M. Pointer, and M. N. Sweeting, "Antennas for modern small satellites" *IEEE Antennas and Propagation Magazine*, Vol. 51, No. 4, pp. 40–56, Aug. 2009

[6] C. G. Kakoyiannis and P. Constantinou "A compact microstrip antenna with tapered peripheral slits for CubeSat RF Payloads at 436MHz: Miniaturization techniques design & numerical results" *Proceedings of the IEEE International Workshop on Satellite and Space Communications (IWSSC 2008*), pp. 255–259, Toulouse, France, Oct. 2008.

[7] O. J. Glasser and J. D. Krauss, "Measured Impedances of Helical Antennas", *J. App Phys*, vol19, Feb 1948, 193-197.

[8] J. D. Kraus "The Helical Antenna," *Antennas, McGraw-Hill*, New York, 1950.

[9] R. L. Carrel, "The Design of Log-Periodic Dipole Antennas", *IRE Int. Conv. Rec.*, vol 9, March 1961.

[10] J. Volakis, "Antenna Engineering Handbook 4th Ed.", *McGraw-Hill*, New York, 2007.

[11] A. Goldsmith, "Wireless Communications", *Cambridge University Press*, New York, NY, 2005.

[12] R. Nugent, R. Munakata, A. Chin, R. Coelho, and J. PuigSuari, "The cubesat: The picosatellite standard for research and education" *AIAA SPACE 2008 Conference and Exposition*, 2008.

[13] J. Dyson, "The Characteristics and Design of the Conical Log-Spiral Antenna", *IEEE Transactions on Antennas and Propagation*, vol 13, July 1965, pp 488-499.

[14] J. Dyson and P. Mayest, "New Circularly-Polarized Frequecn-Independent Antennas with Concial Beam or Omnidirectional Patterns", *IRE Transactions on Antennas and Propagation*, July 1960, pp 334-342.

[15] T. Milligan, " Modern Antenna Design" *Wiley-IEEE Press*, 2nd Edition, 2005.

[16] C. Paul, "Introduction to Electromagnetic Compatibility", *John Wiley and Sons*, Inc., 2nd Edition, New Jersey, 2006.

[17] K. Ang and Y. Leong, "Converting Baluns Into Broad-Band Impedance-Transforming 180° Hybrids", *IEEE Transactions on Microwave Theory and Techniques*, vol 50, August 2002.

[18] C. A. Balanis, "Advanced Engineering Electromagnetics", *John Wiley & Sons*, Hoboken, NJ, 1989.

[19] D. M. Pozar, "Microwave Engineering 3rd Ed", *John Wiley & Sons*, Hoboken, NJ, 2005.

[20] Getting Started, CST Microwave Studio, 2010

[21] Workflow and Solver Overview, CST Microwave Studio, 2010

[22] A. Taflove and S. C. Hagness, "Computational Electrodynamics: The Finite-Difference Time-Domain Method 3rd Ed", *Artech House*, Noorwood, MA, 2005.

[23] Technical Articles RT 5.3.1, "Rogers RT/duroid Material Provides Fexible Substate in New Conical Antenna", *Rogers Corporation: Microwave Materials Division*, Chandler AZ, 1998.

[24] T. Apostol and M. Mnatsakanian, "Unwrapping Curves from Cylinders and Cones", *The Mathematical Association of America*, Monthly 114 May 2007.

[25] R. S. Khandpur, "Printed circuit boards: design, fabrication, assembly and testing*"*, *Tata-McGraw Hill*, 2005, pages 373-378.

[26] Anaren, "Ultra Low Profile 805 Balun 50Ω to 50Ω Balanced", Model BD2130J5050AHF Data Sheet.

[27] Double Ridge Guide Horn Antenna Model: SAS-571, 1 Meter Gain Measurement, AH Systems Inc, Chatsworth, CA, 2009.